

6-17-2004

Analysis and Evolution of Balance In Unstable Barotropic Jets

Travis Allen Smith

Florida State University

Follow this and additional works at: <http://diginole.lib.fsu.edu/etd>

Recommended Citation

Smith, Travis Allen, "Analysis and Evolution of Balance In Unstable Barotropic Jets" (2004). *Electronic Theses, Treatises and Dissertations*. Paper 1666.

THE FLORIDA STATE UNIVERSITY
COLLEGE OF ARTS AND SCIENCES

ANALYSIS AND EVOLUTION OF BALANCE IN UNSTABLE BAROTROPIC JETS

By

TRAVIS ALLEN SMITH

A Thesis submitted to the
Department of Meteorology
in partial fulfillment of the
requirements for the degree of
Master of Science

Degree Awarded:
Summer Semester, 2004

The members of the Committee approve the thesis of Travis A. Smith defended on June 17, 2004.

Philip Cunningham
Professor Directing Thesis

Albert I. Barcilon
Committee Member

T. N. Krishnamurti
Committee Member

The Office of Graduate Studies has verified and approved the above named committee members.

ACKNOWLEDGEMENTS

I would like to sincerely thank my mother and father, Lewis and Rebecca Smith and to my brother, Derrick, for their wonderful love and support throughout my entire life. I especially want to thank my major professor, Dr. Philip Cunningham, for all of his help and guidance through the years and to my committee members, Dr. Albert I. Barcilon, whom has always encouraged me, and Dr. T. N. Krishnamurti. I also want to especially thank my wonderful fiancée, Jessica Stroupe, for the strength, love and encouragement she has given me throughout the years and to all my other friends and family that I have given me wonderful support, including the Cunningham lab. This research was supported by NSF Grant ATM-0120333, awarded to the Florida State University.

This thesis is dedicated to my late grandmothers, Ruby Fox, who saw my love for meteorology as a child, and Novenia Smith.

TABLE OF CONTENTS

List of Tables	vii
List of Figures.....	viii
Abbreviations and Acronyms	x
Abstract.....	xii
Chapter 1. INTRODUCTION.....	1
Chapter 2. MODEL AND DIAGNOSTIC CALCULATIONS.....	8
2.1 Shallow-water model	8
2.2 Rossby and Froude numbers including the “Gamma” parameter.....	11
2.3 Lagrangian Rossby number	11
2.4 Potential vorticity inversion.....	12
2.5 Methodology of study	17
Chapter 3. RESULTS.....	18
3.1 Local Rossby and Froude numbers.....	21
3.2 Ratio of divergence to absolute vorticity, including the“Gamma parameter”	24
3.3 Lagrangian Rossby number	26
3.4 Divergence and diverence tendency	27
3.5 Basic jet evolution and PV inversion.....	28
Chapter 4. SUMMARY AND CONCLUSIONS.....	59

REFERENCES	64
BIOGRAPHICAL SKETCH	69

LIST OF TABLES

I.	Shallow-water model characteristics	10
II.	Ro_J and Fr_J for various initial jet parameters U_o (maximum wind speed) and y_o (jet width).....	17
III.	Summary of all diagnostic calculations and PV inversion results for each simulation.....	57

LIST OF FIGURES

1.	Time series of the local Rossby number for (a) $U_o = 20 \text{ m s}^{-1}$, $y_o = 600 \text{ km}$; (b) $U_o = 30 \text{ m s}^{-1}$, $y_o = 450 \text{ km}$; (c) $U_o = 60 \text{ m s}^{-1}$, $y_o = 450 \text{ km}$	22
2.	Time series of the local Froude number for (a) $U_o = 20 \text{ m s}^{-1}$, $y_o = 600 \text{ km}$; (b) $U_o = 30 \text{ m s}^{-1}$, $y_o = 450 \text{ km}$; (c) $U_o = 60 \text{ m s}^{-1}$, $y_o = 450 \text{ km}$	23
3.	Time series of the ratio of maximum horizontal divergence to maximum relative vorticity (γ) for (a) $U_o = 20 \text{ m s}^{-1}$, $y_o = 600 \text{ km}$; (b) $U_o = 30 \text{ m s}^{-1}$, $y_o = 450 \text{ km}$; (c) $U_o = 60 \text{ m s}^{-1}$, $y_o = 450 \text{ km}$	25
4.	Dynamic fields for $U_o = 20 \text{ m s}^{-1}$ and $y_o = 600 \text{ km}$ at $t = 180 \text{ h}$ including: (a) wind speed (m s^{-1}), (b) relative vorticity (s^{-1}), (c) horizontal divergence (s^{-1}), and (d) potential vorticity (s^{-1}). Maximum/minimum values along with contour intervals are indicated for each parameter.	33
5.	As in Fig. (4) but for $t = 240 \text{ h}$	34
6.	As in Fig. (4) but for $t = 300 \text{ h}$	35
7.	As in Fig. (4) but for $t = 360 \text{ h}$	36
8.	Balanced and unbalanced geopotential height ($\text{m}^2 \text{ s}^{-2}$) and horizontal divergence (s^{-1}) plots for $U_o = 20 \text{ m s}^{-1}$ and $y_o = 600 \text{ km}$ at $t = 180 \text{ h}$	37
9.	As in Fig. (8) but for $t = 240 \text{ h}$	38
10.	As in Fig. (8) but for $t = 300 \text{ h}$	39
11.	As in Fig. (8) but for $t = 360 \text{ h}$	40
12.	Dynamic fields for $U_o = 30 \text{ m s}^{-1}$ and $y_o = 450 \text{ km}$ at $t = 260 \text{ h}$ including: (a) wind speed (m s^{-1}), (b) relative vorticity (s^{-1}), (c) horizontal divergence (s^{-1}), and (d) potential vorticity (s^{-1}). Maximum/minimum values along with contour intervals are indicated for each parameter.	41

13. As in Fig. (12) but for $t = 290$ h.....	42
14. As in Fig. (12) but for $t = 320$ h.....	43
15. As in Fig. (12) but for $t = 350$ h.....	44
16. Balanced and unbalanced geopotential height ($\text{m}^2 \text{s}^{-2}$) and horizontal divergence (s^{-1}) plots for $U_o = 30 \text{ m s}^{-1}$ and $y_o = 450 \text{ km}$ at $t = 260$ h	45
17. As in Fig. (16) but for $t = 290$ h.....	46
18. As in Fig. (16) but for $t = 320$ h.....	47
19. As in Fig. (16) but for $t = 350$ h.....	48
20. Dynamic fields for $U_o = 60 \text{ m s}^{-1}$ and $y_o = 450 \text{ km}$ at $t = 90$ h including: (a) wind speed (m s^{-1}), (b) relative vorticity (s^{-1}), (c) horizontal divergence (s^{-1}), and (d) potential vorticity (s^{-1}). Maximum/minimum values along with contour intervals are indicated for each parameter.....	49
21. As in Fig. (20) but for $t = 110$ h.....	50
22. As in Fig. (20) but for $t = 130$ h.....	51
23. As in Fig. (20) but for $t = 150$ h.....	52
24. Balanced and unbalanced geopotential height ($\text{m}^2 \text{s}^{-2}$) and horizontal divergence (s^{-1}) plots for $U_o = 60 \text{ m s}^{-1}$ and $y_o = 450 \text{ km}$ at $t = 90$ h	53
25. As in Fig. (24) but for $t = 110$ h.....	54
26. As in Fig. (24) but for $t = 130$ h.....	55
27. As in Fig. (24) but for $t = 150$ h.....	56

ABBREVIATIONS AND ACRONYMS

$A_{i,j}$	forcing function at some point i, j
β	β -plane
B_J	Burger number for jet
∇	del operator
δ	horizontal divergence
ε	geostrophic imbalance
f	Coriolis parameter
F	value of general variable
Fr	Froude number
Fr_J	Froude number for jet
g	gravitational acceleration constant
γ	ratio of maximum horizontal divergence to maximum relative vorticity
H	average depth
h	free surface depth deviation
IGW	inertia-gravity wave
$J(u, v)$	Jacobian of the horizontal wind
\mathbf{k}	unit vertical vector
m	meter
$m\ s^{-1}$	meter per second
N_δ	nonlinear terms of divergence equation
N_Φ	nonlinear terms of continuity equation
N_ζ	nonlinear terms of vorticity equation
Ω	Earth's rotation velocity
Φ	geopotential height
$\bar{\Phi}$	average geopotential height
ϕ	latitude
PV	potential vorticity
Q	potential vorticity
$R_{i,j}$	residual at some point i, j
Ro	Rossby number
Ro_L	Lagrangian Rossby number

Ro_J	Rossby number for jet
ΔNBE	residual of the nonlinear balance equation
t	time
U	wind velocity
u	u-component of the wind
\mathbf{V}	horizontal wind vector
\mathbf{V}_{ag}	ageostrophic wind vector
v	v-component of the wind
X	general component
y	jet width
ζ	relative vorticity

ABSTRACT

The nature of balance in the atmosphere is of central importance to the dynamics of both the troposphere and the stratosphere, and unbalanced motions such as inertia-gravity waves play a significant role in many aspects of atmospheric behavior. In light of the importance of upper-tropospheric jets for the generation of inertia-gravity waves in the atmosphere, this study examines the evolution of unstable barotropic jets to assess the nature and evolution of balance in these features. This issue is explored using the simplest non-trivial dynamical framework in which balanced and unbalanced flows can coexist, namely the one-layer shallow water equations.

In this study, numerical simulations of initially balanced zonal barotropic jets on an f plane are investigated for evidence of the breakdown of balance and the generation of inertia-gravity waves during the life cycles of the instabilities to these jets. In these simulations, the parameters of the basic-state jet (i.e., jet width and speed) are varied systematically in an attempt to elucidate the dependence of balance on the structure and dynamical evolution of the instability.

The presence of unbalanced flow, either in numerical simulations or in atmospheric data, is typically inferred via various quantities that provide indirect measures of imbalance, such as the existence of strong ageostrophy, large Rossby and/or Lagrangian Rossby numbers, and large values of horizontal divergence and its material derivative. Along with evaluating these parameters in each simulation, a potential vorticity inversion method is employed to obtain the structure of balanced and unbalanced fields within each simulation. The diagnostic calculations are then compared to the potential vorticity inversion results.

Contrasts and comparisons are presented for each of the simulations shown in this study. The simulations consist of an unstable barotropic wave ranging from small (i.e.,

$O(10^{-1})$) Rossby and Froude number to large (i.e., $O(1)$) Rossby and Froude number. For strong jets, neither the Rossby number nor the Froude number is small compared to unity therefore the applicability of traditional scale analysis is unclear (e.g. Haltiner and Williams, 1980) (i.e., the balance condition is no longer valid and a breakdown of balance should occur). In contrast, the results of the diagnostic calculations and potential vorticity inversions reveal that nonlinear balance is essentially valid for this particular jet profile, even though the Rossby and Froude numbers are $O(1)$ for the strong barotropic jet. Significant inertia-gravity wave structures were not found in any of the cases shown here, which is consistent with the results obtained by several other investigators in their integrations of the shallow-water equations.

CHAPTER ONE

INTRODUCTION

The concept of balanced flow is central to dynamic meteorology, and provides the foundation for much of our theoretical and phenomenological understanding of synoptic- and planetary-scale circulations. Balance flow concepts have also been of great importance in the study of numerical modeling and forecasting; the theoretical and practical reason for these concepts has been explored in numerous scientific publications since the first numerical forecasts were performed by Charney (1950).

Understanding atmospheric imbalance has since become a fundamental issue in the realm of numerical modeling. These imbalances are responsible for the generation of inertia-gravity waves (IGWs), and forecasting in the early years of numerical weather prediction was made extremely difficult due to these inherent high-frequency solutions contained in the primitive equations. Pioneering work presented by Charney (1948) showed that atmospheric motions could be approximated by truncating the primitive equations through proper scale analysis. This simplification greatly reduced the problem of forecasting due to the elimination of many small terms, including the high frequency solutions or IGWs. However, the quasi-geostrophic system of equations so obtained, albeit a fair approximation, was sometimes found to eliminate many aspects of the flow important for weather systems and was not suitable for operational forecasting. However, another system of equations that was more general but still eliminated the fast modes was introduced by Charney (1962). This “balanced” system was more accurate in retaining the characteristics of the flow, and has since been modified many times for use in numerical forecasting, and as will be discussed later, for diagnosing the possibility of imbalance in atmospheric data and numerical simulations.

The utility of the balance concept is succinctly expressed in the concept of “potential vorticity (PV) thinking” described by Hoskins et al. (1985). This landmark paper discusses the role of PV in determining dynamical properties of the atmosphere. They state that the “invertibility principle” of PV, given a suitable balance condition, allows for the total mass, wind, and all other dynamical fields to be deduced knowing the global distribution of PV. Balance dynamics and balanced systems of equations also frequently exhibit a degree of accuracy well beyond what is expected in terms of atmospheric phenomena. In this regard, the diagnosis of both observations and primitive equation models using balance equations has been applied successfully to describing aspects of rapidly intensifying extratropical cyclones (e.g., Davis et al. 1996) and mesoscale convective systems (e.g., Davis and Weisman 1994; Olsson and Cotton 1997). In addition, numerical simulations using balanced models have been shown to provide accurate representations of such mesoscale phenomena (e.g., Montgomery and Farrell 1992; Jiang and Raymond 1995). Indeed, Davis et al. (1996, p. 23) assert that “success here strongly motivates the continued use of balance equations to describe phenomena such as jet streaks, straight and curved, and mesoscale aspects of cyclones.”

Despite the demonstrated success of balanced dynamics in understanding and predicting the atmosphere over a wide range of spatial and temporal scales, unbalanced motions are known to play a significant role in many aspects of atmospheric behavior. In particular, gravity waves transport energy and momentum both horizontally and vertically and as such play a crucial role in determining the large-scale circulation in the middle atmosphere (e.g., Matsuno 1982; Holton 1983; Fritts et al. 1984). Also, large-amplitude gravity waves have been found to have a significant impact on the mesoscale dynamics of the troposphere, and it is widely believed that large-amplitude gravity waves are responsible for the initiation and organization of severe weather (e.g., Uccellini 1975; Stobie et al. 1983; Koch et al. 1988).

The potential sources of gravity waves in the atmosphere have received considerable attention in the scientific literature. These sources include topography, convection, and shear instability; IGWs that develop from these sources have relatively high intrinsic frequencies. However, observations indicate that the energy spectrum of gravity wave motions is dominated by waves with low intrinsic frequencies (e.g., Fritts

and Chou 1987; Fritts et al. 1990). These IGWs typically have periods of 3-24 hours, horizontal scales of 200-1000 km, and vertical scales of 1-5 km. Mesoscale gravity waves in the troposphere that are associated with severe weather are frequently of large enough horizontal scale (50-500 km), and of long enough period (1-4 h) to possess characteristics of IGWs (e.g., Bosart et al. 1998; Koppel et al. 2000).

There is evidence, both from observations (e.g., Hirota and Niki 1986; Fritts et al. 1998; Guest et al. 2000) and numerical simulations (e.g., O'Sullivan and Dunkerton 1995; Bush et al. 1995; Charron and Brunet 1999; Zhang 2004), to suggest that IGWs in the stratosphere are generated in the vicinity of jet-front systems in the upper troposphere. Moreover, jet-front systems appear to be an essential component of the synoptic-scale environment identified as being conducive to IGW generation in the troposphere. Uccellini and Koch (1987) described the typical synoptic-scale environment in which IGWs develop and propagate through the troposphere. A review of thirteen mesoscale IGW case studies revealed that these IGW events were associated with a distinct synoptic pattern. Specifically, tropospheric IGWs typically develop between the exit region of an upper-tropospheric jet streak and a downstream upper-level ridge axis in a statically-stable region north of a surface warm frontal boundary. This synoptic-scale configuration also appears to be important for IGWs in the stratosphere, as seen in observations (e.g., Guest et al. 2000) and numerical simulations (e.g., O'Sullivan and Dunkerton 1995; Zhang 2004).

The majority of the literature concerning the generation of IGWs by the aforementioned jet-front systems discusses the role of geostrophic adjustment in the presence of unbalanced flow (e.g., Van Tuyl and Young 1982; Uccellini and Koch 1987; Zack and Kaplan 1987; Koch and Dorian 1988). The presence of unbalanced flow has been inferred via various quantities that provide indirect measures of imbalance, such as the existence of strong ageostrophy, large Rossby and/or Lagragian Rossby numbers, and large values of horizontal divergence and its material derivative. However, these quantities are based on specific balance constraints (i.e., quasigeostrophy, semigeostrophy, or nonlinear balance), and it should be noted that an assessment of balance based on the inaccuracy of these constraints allows for the possibility that the “unbalanced flow” so identified includes higher-order balanced motions not accounted

for in the system under consideration in addition to IGWs. Indeed, not only does the possibility exist that balanced flows may possess large Rossby (Ro) and large Lagrangian Rossby numbers (Ro_L), but it is also possible to construct high-order balanced systems in which the divergence tendency is nonzero (e.g., McIntyre and Norton 2000), which implies the existence of higher-order balanced states not well described by the nonlinear balance equation. Consequently, it is suggested that the above quantities should be interpreted as approximate indicators, and not as absolute measures of the presence of unbalanced flow.

Although previous idealized investigations of the generation of IGWs in jet-front systems have examined geostrophic adjustment associated with unbalanced initial conditions (e.g., Van Tuyl and Young 1982; Fritts and Luo 1992; Luo and Fritts 1993; Weglarz and Lin 1997), Fritts (1993, p. 201) notes that “in principle, a full description of the wave field arising from geostrophic adjustment should account for the gradual evolution of the unbalanced state.” Despite this important admission, few studies have considered the processes by which initially balanced jet-front systems evolve towards a state of imbalance (e.g., Van Tuyl and Young 1982; Bush et al. 1995; O’Sullivan and Dunkerton 1995; Zhang 2004), emitting IGWs as they do so. In Van Tuyl and Young (1982), studies of a baroclinic jet with both balanced and unbalanced initial conditions are performed. In both cases, they found that the unbalanced motions forced by the jet were found to be persistent in both time and space, and comprised of a gravity-inertia signal with amplitude depending on the Rossby number. However, a model using higher resolution would have allowed for the examination of more intense jet streaks and significant differences in the unbalanced components as the Rossby number approached unity.

Insight into the generation of IGWs from a balanced antecedent state may be provided by the extensive literature concerning balanced dynamics, and in particular that concerning the so-called “slow manifold” (e.g., Leith 1980; Lorenz 1980). A slow manifold is conjectured as a manifold of the phase space which is invariant under the dynamics and on which the flow is devoid of high frequency oscillations, and if an exact slow manifold were to exist, a flow initially in balance would be expected to remain so for all time. There are convincing arguments against the existence of an exact slow

manifold, based on both analytical and numerical evidence indicating that IGWs, when admissible solutions to the governing equations, are almost always present to some degree regardless of whether the initial state is balanced or not (e.g., Errico 1982; Vautard and Legras 1986; Warn 1986, 1997; Warn and Menard 1986).

From the perspective of a scale analysis (e.g., McWilliams 1985; Spall and McWilliams 1992; McIntyre and Norton 2000), it is required that either the Rossby number or the Froude number be small for nonlinear balance to be valid; however, neither of these conditions are met for strong jets. Spall and McWilliams (1992) present a scale analysis for the shallow-water equations over a large range of Rossby and Froude numbers, and found that unbalanced motions remain quite small even for very large Rossby numbers when the Froude number is small. As the value of the Froude number increased, they found that the solutions moved either toward non-existence of balance or a regime of non-balance; however, they were unable to formally make a conclusion for very large Rossby and Froude numbers. Bush et al. (1995) study an unstable *baroclinic* wave, and found that scaling assumptions based on nonlinear balance formally break down during the life cycle of the wave. They studied both the slow synoptic-scale development of the baroclinic wave and the mesoscale frontal regime to which the flow collapses and found that both slow and fast unbalanced motions occur. However, the barotropic dynamics for large Rossby and Froude number regimes for jets have not been extensively studied and presented in the literature. Ford (1994) presented a study on gravity wave radiation by vortical flows in the f plane shallow-water equations. In each simulation, the initial flow consisted of two jets flowing in opposite direction. The resulting strip of PV was examined through its nonlinear evolution as vortices developed and subsequently radiated IGWs. However, Ford specifically examined the far-field region for the evidence of IGWs, while this study specifically looks for evidence of IGWs in the near-field (i.e., in the jet region).

Mohebalhojeh and Dritschel (2000) recently studied the generation of IGWs in numerical models of the shallow-water equations using the CASL (contour-advection semi-Lagrangian) method to assess the generation of gravity waves. They present a hierarchy (similar to McIntyre and Norton (2000)) of shallow-water equations for use with the CASL algorithm to implement PV inversion. They compare and contrast each

CASL algorithm to determine their accuracy in representing IGWs in the model simulation. Specifically, implementation of the contour-advection algorithm requires that each contour on a given surface or field must be represented by a variable number of computational points or nodes spaced according to a function of contour curvature. Each node is then advected by a velocity that is interpolated from the gridded data. As a result, the CASL algorithm allows one to see fine-scale features that are invisible in an instantaneous grid-generated picture of the field (Ditchel and Ambaum 1999).

Despite the theoretical interest in the dynamics of balanced-unbalanced interactions, and the evidence for the role of jet-front systems in generating IGWs, there does not appear to have been a systematic idealized investigation of the evolution of balance and the generation of unbalanced flow in jet-front systems, either from the perspective of the nature of the evolution of the jet-front system itself, or from the perspective of the dependence of IGW generation on suitably defined Rossby and Froude numbers. Also, despite the proliferation of numerical studies of the life cycles of unstable baroclinic waves, investigations into the generation of unbalanced flow in baroclinic-wave life cycle simulations have been relatively rare (e.g., Whitaker 1993; Bush et al. 1995; O’Sullivan and Dunkerton 1995; Zhang 2004), most likely because the bulk of evidence indicates that baroclinic waves are well described by balanced models. Subsequently, barotropic-wave life cycle simulations have not been presented in literature in regards to the generation of unbalanced flow with the exception of Ford (1994), although he considered shear layers (PV strips). Of particular relevance and importance to the present study is the ideal property that gravity waves are absent from the initial state in such simulations, and thus any subsequent generation must be due to the internal dynamics of the evolving flow, assuming that spurious numerical generation of IGWs has been ruled out.

In light of the importance of upper-tropospheric jets for the generation of IGWs in the atmosphere, this study examines the evolution of unstable barotropic jets to assess the nature and evolution of balance of these features. This issue is explored using the simplest non-trivial dynamical framework in which balanced and unbalanced flows can coexist, namely the one-layer shallow-water equations.

In this study, numerical simulations of initially balanced zonal barotropic jets on an f plane are investigated for evidence of the breakdown of balance and the generation of IGWs during the life cycles of the instabilities to these jets. In these simulations, the parameters of the basic-state jet (i.e., jet width and speed) are varied systematically in an attempt to elucidate the dependence of balance on the structure and dynamical evolution of the instability. This produces a study with a wide range of Rossby and Froude numbers to obtain qualitative and quantitative understanding of balanced and unbalanced motions of this specific jet profile. In strong jets, neither the Rossby number nor the Froude number are small compared to unity, therefore the applicability of traditional scale analysis is unclear. These jets are the focus of this thesis, and it will be shown that unbalanced motions in these jets are extremely small and that IGWs of large amplitude are not generated in shallow-water model simulations. This study examines the various diagnostic quantities mentioned previously, in addition to a PV inversion to better quantify the existence of unbalanced flow in the barotropic shallow-water equation model. The method utilized for the PV inversion is derived from a set of equations called the “slow equations” introduced by Lynch (1989), but has many similarities to the method described by McIntyre and Norton (2000).

The thesis is presented in several chapters, highlighting each calculation and their results. Chapter 2 describes the one-layer shallow water model and details the diagnostic calculations to be performed in each simulation along with the methodology of the study. Chapter 3 presents the results of the study by providing the evolution of each diagnostic calculation and an extensive discussion of their relevance to balance concepts. Finally, Chapter 4 presents the conclusions and possible future work in the area of unbalanced motions and IGWs.

CHAPTER TWO

MODEL AND DIAGNOSTIC CALCULATIONS

2.1 Shallow-Water Model

The one-layer barotropic shallow-water model is the simplest non-trivial dynamical framework in which balanced and unbalanced flows can coexist. The model is governed by the shallow-water equations, given by

$$\frac{\partial u}{\partial t} + u \frac{\partial u}{\partial x} + v \frac{\partial u}{\partial y} - fv = -\frac{\partial h}{\partial x} \quad (1)$$

$$\frac{\partial v}{\partial t} + u \frac{\partial v}{\partial x} + v \frac{\partial v}{\partial y} + fu = -\frac{\partial h}{\partial y} \quad (2)$$

$$\frac{\partial h}{\partial t} + u \frac{\partial h}{\partial x} + v \frac{\partial h}{\partial y} = -(H + h) \left(\frac{\partial u}{\partial x} + \frac{\partial v}{\partial y} \right). \quad (3)$$

Equations (1) and (2) are the horizontal x - and y -momentum equations and (3) is the continuity equation. The variables u and v are the horizontal components of the wind, f is the Coriolis parameter, and h is the free surface deviation from a constant mean depth, H .

For simplicity, an f -plane geometry ($\beta = 0$) is chosen for the Coriolis parameter, such that $f = f_o$, where $f_o = 2\Omega \sin \phi$, Ω is the angular speed of the earth's rotation, and ϕ is the central latitude of the computational domain. The central latitude is chosen

to be 40°N (representative of the midlatitudes), and thus f_o is $9.37 \times 10^{-5} \text{ s}^{-1}$. The model is utilized to simulate the life cycles of the instabilities to the basic-state zonal profile

$$U(y) = U_o \operatorname{sech}^2 \left(\frac{y}{y_o} \right), \quad (4)$$

where U_o is the maximum jet speed (m s^{-1}), and y_o is the jet width (m). The jet profile (4) is known as the Bickley jet. Westerly jets ($U_o > 0$) in the upper levels of the troposphere can be represented by the Bickley jet. Random perturbations of infinitesimal amplitude are added to this basic-state jet, and the model is run to grow an unstable wave. Boundary conditions in x are periodic and in y are solid wall with a damping layer to prevent reflection of IGWs back into the domain. A coordinate transformation is used in the y direction so that boundaries are far from the jet region. The domain length for each simulation is equal to one wavelength of the most unstable mode. The most unstable wavelength is found by systematically changing the domain length for a certain jet width and calculating the growth rate as the wave grows. The domain width for every simulation is 6000 km. The depth of the layer is 750 m with a constant density normalized to a value of 1.0.

The shallow-water equations (1)-(3) are solved numerically using a finite-difference representation described by Arakawa and Lamb (1981) that conserves total energy (i.e., kinetic plus potential) and potential enstrophy. Enstrophy conservation is important since the atmosphere is quasi-nondivergent, and Arakawa (1966) argued that conservation of energy and enstrophy in a barotropic model precludes false transfer of energy to smaller scales. A leapfrog time differencing scheme is employed with a weak time filter to reduce high-frequency noise. A biharmonic spatial filter with damping coefficient of $1 \times 10^{11} \text{ m}^4 \text{ s}^{-1}$ is used to control nonlinear instability and aliasing. All figures in this thesis define $t = 0 \text{ h}$ as the point in which the v -component of the wind reaches 1 m s^{-1} . The model is summarized in Table I.

Diagnostic Calculations

2.2 Nondimensional numbers including the “Gamma” parameter

Table I. Shallow-water model characteristics.

Shallow-Water Model Characteristics	
No. of Layers:	1 (barotropic)
Coriolis:	f-plane
Solving Method:	centered finite differences
Grid:	staggered (C-grid)
Boundary Conditions:	periodic in x solid wall in y with damping layer
Layer Depth:	750 m
Central Latitude:	40 degrees North
Time Step:	20 s
Domain Size:	6000 km in y 2900 km in x for jet width 450 km 3500 km in x for jet width 600 km
Grid Spacing:	10 km
Gravitational Constant:	9.80665 m s^{-2}
Biharmonic Damping Coefficient:	$10^{-10} \text{ m}^4 \text{ s}^{-1}$

To begin this study, a survey of unbalanced flow diagnostics are performed on each simulation in an initial effort to quantify the degree of imbalance found in each unstable wave as it grows to finite amplitude and beyond. Again, imbalance is defined in terms of what extent the flow departs from a specific balanced state and several methods have been formulated to attempt to quantify the presence of unbalanced flow. In order to attempt to perform IGW analysis, it is important than no IGWs are present at the start of the model integration. A description of each diagnostic calculation follows with the results to be presented in the next chapter.

Associated with the jet profile, (4), it is possible to define Rossby and Froude numbers for the jet as follows

$$Ro_J = \frac{U_o}{f_o y_o} , \quad Fr_J = \frac{U_o}{\sqrt{gH}} . \quad (14)$$

In addition, it may be useful to consider local values of Ro and Fr , defined by

$$Ro = \frac{\zeta_{\max}}{f_o} \quad \text{and} \quad Fr = \frac{|\mathbf{V}|}{\sqrt{gh}} \quad (15)$$

where ζ_{\max} is the maximum relative vorticity in the domain. Also, we can define a parameter, γ ,

$$\gamma = \frac{\delta_{\max}}{\zeta_{\max}} , \quad (16)$$

where δ_{\max} is the maximum horizontal divergence in the domain. This parameter provides a crude estimate of the validity of nonlinear balance following the ad hoc scale analysis of Haltiner and Williams (1985).

2.3 Lagrangian Rossby number

The Lagrangian Rossby number is a quantity in which the ratio of parcel acceleration to Coriolis acceleration is calculated in terms of the ageostrophic wind (Van Tuyl and Young 1982). The Lagrangian Rossby number is defined as

$$Ro_L = \frac{|d\mathbf{V}/dt|}{f_o |\mathbf{V}|} . \quad (17)$$

The frictionless equation of motion is defined as

$$\frac{d\mathbf{V}}{dt} = f_o \mathbf{V}_{ag} \times \mathbf{k}. \quad (18)$$

therefore, Ro_L can then be defined as

$$Ro_L = \frac{|k \times f \mathbf{V}_{ag}|}{f |\mathbf{V}|} = \frac{|\mathbf{V}_{ag}|}{|\mathbf{V}|}. \quad (19a)$$

Ro_L becomes a measure of ageostrophy which is the departure from geostrophic balance. Van Tuyl and Young (1982) found that values of the computed Ro_L that exceeded 0.5 in a region where $|\mathbf{V}| > 10 \text{ m s}^{-1}$ indicated a region of unbalanced flow. They found these particular values at and downwind of the core of maximum jet wind speeds. An even more exact method of estimating the Ro_L to measure the degree of imbalance defined by Koch and Dorian (1988) is:

$$Ro_L = \frac{|\mathbf{V}_{ag}^\perp|}{|\mathbf{V}|}. \quad (19b)$$

The ratio of the ageostrophic wind perpendicular to the flow to the total wind is used because they assumed that the alongstream ageostrophic wind should be governed by gradient wind balance. They proposed that the cross-stream ageostrophic flow directed toward the cyclonic side of the jet should be used to assess unbalanced flow. This quantity is useful only when (19a) is deemed large enough to indicate a possible unbalanced flow region.

2.4 Potential vorticity inversion

Potential vorticity inversion is used as a diagnostic tool to determine regions of unbalanced flow in each simulation. The PV inversion is formulated using the method of Lynch (1989), in which the fast modes are filtered out of the shallow-water equations (Lynch aptly names this system the “Slow Equations”). The slow equations are first derived by taking the curl ($\nabla \times$) and the divergence ($\nabla \cdot$) of the horizontal momentum equations and formulating the continuity equation in terms of divergence. The resulting equivalent shallow-water system is,

$$\frac{\partial \zeta}{\partial t} + f_o \delta = -N_\zeta \quad (20)$$

$$\frac{\partial \delta}{\partial t} - f_o \zeta + \nabla^2 \Phi = -N_\delta \quad (21)$$

$$\frac{\partial \Phi}{\partial t} + \bar{\Phi} \delta = -N_\Phi \quad (22)$$

where $\delta = \frac{\partial u}{\partial x} + \frac{\partial v}{\partial y}$ is the horizontal divergence, $\zeta = \frac{\partial v}{\partial x} - \frac{\partial u}{\partial y}$ is the relative vorticity, $\Phi = gh$ is the geopotential, $\bar{\Phi} = gH$ is the average geopotential, and the

N 's are the nonlinear terms of each equation. These nonlinear terms are defined as

$$N_\zeta = \mathbf{V} \cdot \nabla \zeta + \zeta \delta, \quad (23)$$

$$N_\delta = \mathbf{V} \cdot \nabla \delta + \delta^2 - 2J(u, v), \quad (24)$$

$$N_\Phi = \mathbf{V} \cdot \nabla \Phi + (\Phi - \bar{\Phi}) \delta, \quad (25)$$

where J is the Jacobian operator, $J(u, v) = \left(\frac{\partial u}{\partial x} \frac{\partial v}{\partial y} - \frac{\partial u}{\partial y} \frac{\partial v}{\partial x} \right)$. Combining the vorticity and

continuity equations yields the conservation of shallow-water PV:

$$\frac{d}{dt} \left(\frac{\zeta + f_o}{\Phi} \right) = 0. \quad (26)$$

The linear eigenmodes of the system (20)-(22) show that the slow modes are stationary, geostrophic, and nondivergent. It can also be shown that the fast modes have zero linearized PV. The fast modes must have non-zero frequencies; therefore, these properties imply that divergence tendency and the geostrophic imbalance tendency (to be discussed shortly) project entirely onto the fast modes (the raised dot denotes time tendency). The PV tendency, on the other hand, projects entirely onto the slow modes. Separating the time tendencies into slow and fast components gives:

$$\frac{\partial X}{\partial t} = \frac{\partial X_R}{\partial t} + \frac{\partial X_G}{\partial t}, \quad (27)$$

where subscript R denotes the Rossby modes or slow modes, and subscript G denotes the gravity wave modes or fast modes. An imbalance equation can be derived and used to eliminate the gravity wave modes from (20) and (22). Taking ∇^2 of the continuity equation and multiplying the vorticity equation by f_o and subtracting the two equations yield

$$\nabla^2 \dot{\Phi} - f_o \dot{\zeta} + \nabla^2 (\overline{\Phi} \delta) - f_o^2 \delta = -\nabla^2 N_\Phi + f_o N_\zeta. \quad (28)$$

Rearranging (28) yields

$$\dot{\varepsilon} + \left(\nabla^2 - \frac{f_o^2}{\Phi} \right) \overline{\Phi} \delta = -(\nabla^2 N_\Phi - f_o N_\zeta), \quad (29)$$

where $\dot{\varepsilon} = \nabla^2 \Phi - f_o \zeta$ is the geostrophic imbalance tendency. Using (29) in conjunction with (26), PV conservation, and with (21), the divergence equation, gives a system equivalent to (20)-(22). Assuming that gravity wave projections of time tendency vanish yields

$$\frac{d}{dt} \left(\frac{\zeta + f_o}{\Phi} \right) = 0, \quad (30)$$

$$\nabla^2 \Phi - f_o \zeta = -N_\delta, \quad (31)$$

$$\left(\nabla^2 - \frac{f_o^2}{\Phi} \right) \overline{\Phi} \delta = -(\nabla^2 N_\Phi - f_o N_\zeta), \quad (32)$$

which are the “Slow Equations”. Combining the definition of PV and (21) yields an equation for the geopotential,

$$\left(\nabla^2 - \frac{f_o^2}{\Phi} \right) \Phi = -N_\delta - f_o^2 + f_o \left\{ Q - \left(\frac{f}{\Phi} \right) \right\} \Phi, \quad (33)$$

where Q is the PV. Equations (32) and (33) are two Helmholtz equations used to implement the PV inversion. The slow system contains one prognostic equation (conservation of PV). The diagnostic elements of the system are (31) and (32), in which the divergence tendency and geostrophic imbalance have been eliminated. Equation (31)

is the nonlinear balance equation; therefore, the balance condition (i.e. nonlinear balance) is explicitly specified in the slow equations.

It is necessary that boundary conditions must be specified in order to solve each Helmholtz equation. As stated above, periodic boundary conditions are used on the x -boundaries; however, the boundary conditions in y are different for each Helmholtz equation. For (33), a Neumann boundary condition specifying the geopotential gradient along the boundary is utilized, which is

$$\frac{\partial \Phi}{\partial y} = f_o u. \quad (34)$$

This geostrophic boundary condition is appropriate for the retrieval of the balanced flow from the initial data. . For Eq. (32), the Dirichlet boundary condition is

$$\delta = 0, \quad (35)$$

i.e., horizontal divergence is zero on the y boundaries. Each Helmholtz equation is then solved iteratively via relaxation.

The PV inversion resultant from the slow system of equations is straightforward; however, the solution must be found iteratively by solving (32) and (33). The most important concept concerning the PV inversion is that the PV field remains the same (i.e., not updated) over the course of the PV inversion. First, for each time in the simulation in which the PV inversion is applied, the height and u, v components of the wind are recorded. From this data, the initial fields for the PV inversion (geopotential, divergence, and PV) are calculated. These initial fields are then utilized to solve the Helmholtz equation (33) for Φ on the LHS using the initial geopotential field as the first guess in the terms on the RHS to obtain the balanced geopotential (Φ_b). Φ_b is then used to solve (32) using the initial divergence field as the first guess in the terms on the RHS to solve for the new balanced divergence (δ_b) (δ on the LHS). Again, each Helmholtz equation is solved separately by iteration to obtain the balanced fields, Φ_b and δ_b . Subsequently a new balanced relative vorticity field can be obtained from the definition of PV as follows,

$$\zeta_b = \Phi_b Q - f_o. \quad (36)$$

By subtracting the balanced fields from the initial fields, the unbalanced portion of the fields is obtained.

After solving for Φ_b and δ_b , it is then necessary calculate the new balanced winds from these values. Using well-known vector identities, the wind can be written as

$$\nabla^2 \mathbf{V} = \nabla \delta + \mathbf{k} \times \nabla \zeta \quad (37)$$

Equation (37) indicates that given the divergence and vorticity fields, this vector Poisson equation can be solved for \mathbf{V} if the velocity on the boundaries is specified. However, to implement this method to obtain convergence of this Poisson equation (following Lynch 1989), it is necessary to solve each component of the wind separately. Taking (37), one can rewrite the equation in component form:

$$\nabla^2(u\mathbf{i}+v\mathbf{j})=\left(\frac{\partial\delta}{\partial x}-\frac{\partial\zeta}{\partial y}\right)\mathbf{i}+\left(\frac{\partial\delta}{\partial y}+\frac{\partial\zeta}{\partial x}\right)\mathbf{j}. \quad (38)$$

Therefore, each component of the balanced wind can be specified as

$$\nabla^2 u_b = \frac{\partial \delta_b}{\partial x} - \frac{\partial \zeta_b}{\partial y} \quad (39)$$

and

$$\nabla^2 v_b = \frac{\partial \delta_b}{\partial y} + \frac{\partial \zeta_b}{\partial x}. \quad (40)$$

After obtaining the new balanced wind field components u_b and v_b , Φ_b and δ_b are recalculated starting from (33) and (32) using the new balanced geopotential and wind components. It is critical to remember the PV field is considered to be given, and is not updated with each successive iteration to obtain the balanced and unbalanced fields. Generally, flows with small imbalances only require one or at most two iterations of the slow equation system to obtain the most accurate solution while larger imbalances may need several iterations of the entire system.

2.5 Methodology of Study

Using the one-layer shallow water model, three simulations are shown to illustrate the degree of balance obtained from the diagnostic calculations. Each simulation begins with an initially balanced jet and the simulation is run until the barotropic wave is well

developed. The initial jet parameters vary for each simulation (i.e. Ro_J and Fr_J are chosen to be different) to produce three simulations in which comparisons and contrasts are deduced. The role of this “matrix” of Ro_J and Fr_J numbers and its effects on the balanced and unbalanced flow is the premise for this thesis.

The initial Ro_J and Fr_J numbers for each simulation are shown in Table I. U_o and y_o are chosen carefully in order to produce simulations in which there are a wide range of Rossby and Froude numbers.

Table II. Ro_J and Fr_J for various initial jet parameters
 U_o (maximum wind speed) and y_o (jet width).

U_o (m s^{-1})	y_o (km)	Ro_J	Fr_J
20	600	0.20	0.17
30	450	0.70	0.35
60	450	1.42	0.70

The diagnostic calculations (i.e. Ro_J , γ , PV inversions, etc.) are performed for each simulation and are discussed based on their role in determining whether unbalanced flow and IGWs are present.

CHAPTER THREE

RESULTS

An important and ubiquitous issue in the study of jets and jet streaks concerns the degree of balance associated with these features. In this study, we attempt to clarify better whether the barotropic, shallow-water equation model is capable of producing large unbalanced motions and subsequent IGW activity. However, the fundamental question which many investigators have attempted to answer: What is the definition of balance?

A definition of balance based on the accuracy of a balance relation (e.g. geostrophic or nonlinear balance) will not be unique. Given this ambiguity, we proposed the following definition that, although imprecise, is entirely consistent with recent research concerning balanced dynamics: a given flow may be considered to be balanced provided that the IGWs that are present are of sufficiently small amplitude that they do not affect the flow evolution. The goal of balanced dynamics is to reduce the primitive equations in order to develop a set of equations that filters the ‘fast’ inertia-gravity oscillations, and thus describes the ‘slow’ evolution of the system. The balanced systems so derived often are employed as predictive models in place of the primitive equation system or as simplified sets of equations to gain basic understanding of certain phenomena.

Much of the recent investigation of balanced dynamics has centered on the concept of the ‘slow manifold’ (Leith 1980; Lorenz 1980). The idea underlying this concept is that rather than occupying the entire phase space of all possible flow states in the primitive equations, the flow states that may be realized are constrained to a lower-dimensional manifold within the phase space, and these flow states describe the slow (i.e. balanced) evolution. The existence of a slow manifold is equivalent to the existence of an exact balance relation, which may be of higher order than geostrophic or nonlinear

balance (termed ‘superbalance’) by Lorenz (1980)), such that flows initially in such balance remain so for all time. Leith (1980) suggests that, if given initial conditions on the slow manifold, the subsequent evolution will display oscillations about it that damp with time in association with the geostrophic adjustment process.

The slow manifold and superbalance concepts are useful, since they promote the awareness that a given balance relation may not describe entirely the balanced flow. Nevertheless, a number of investigations have asserted that the slow manifold does not exist, or exists only in an approximate sense (e.g. Errico 1984; Vautard and Legras 1986; Warn 1997) and, moreover, that the utility of the slow manifold concept decreases with increasing Rossby number. Support for this assertion comes for the findings of Sadourny (1975), Errico (1982, 1984), Warn (1986), Warn and Menard (1986), and Bartello (1995), which suggest that inertia-gravity waves almost always are present at some amplitude in primitive equation flows, even in the limit of small Rossby numbers and long times. Nevertheless, in such cases that flow may still be regarded as balanced provided that the inertia-gravity waves present are of sufficiently small amplitude (Warn 1997).

Van Tuyl and Young (1982) show that IGWs are generated in a baroclinic two-layer primitive equation model in a region of unbalanced flow near the jet core, where the criteria needed to apply the balance equation are not satisfied. The amplitude of the unbalanced motion increases with the square of the Rossby number, particularly around and immediately downwind of the jet core. They attributed these motions to the geostrophic adjustment process. Geostrophic adjustment occurs when an unbalanced mass and momentum field restores itself to geostrophic balance by releasing IGW (Blumen, 1972). For sufficiently high Rossby numbers, such as those encountered near strong jet streaks, Van Tuyl and Young (1982) suggest that secondary circulations predicted by quasi-geostrophic and balance theories would be unable to maintain the balance condition that initially exists. Therefore, IGW, or related unbalanced motions, should result. Subsequently, a considerable number of investigations after Van Tuyl and Young (1982) have categorized jet streaks as unbalanced flow phenomena, asserting that the process of geostrophic adjustment and the presence of inertia-gravity waves may be common to these features in the atmosphere (e.g. Kaplan and Paine 1977; Van Tuyl and Young 1982; Uccellini and Koch 1987; Kaplan et al. 1997; Weglarz and Lin 1997). As

discussed in the Introduction, Uccellini and Koch (1987) identified the flow configuration that is particularly conducive to the generation of inertia-gravity waves: a jet stream in southwesterly flow approaching a ridge axis. It is commonly hypothesized that such a configuration presents a situation in which the divergence tendency becomes large and the nonlinear balance equation is no longer valid (Kaplan and Paine 1977).

To investigate the evolution of balance in the barotropic jet structure, we calculate and show the evolution of each diagnostic calculation discussed in Chapter 2. Each barotropic simulation will be run to some finite amplitude to a point where jet streaks are present within the structure of the jet and beyond. Then the following calculations are investigated for their magnitude and structure:

(i) The local Rossby and Froude numbers are examined in relation to scale analysis presented by several investigators.

(ii) The next step is to evaluate the magnitude of the horizontal divergence relative to the magnitudes of the total relative vorticity. The ratios obtained provide initial estimates of the contribution of the divergence to the total flow. If large, these ratios may indicate the possibility of imbalance in the flow under consideration.

(iii) The divergence tendency is examined to determine if its magnitude may be significant for imbalance to develop.

(iv) The Lagrangian Rossby number, Ro_L , is calculated to determine the magnitude of the ageostrophic flow to the total flow. Strong ageostrophy is a very good indicator where the flow may be unbalanced.

(v) Finally, there remains an attempt to identify the respective contributions from the balanced and unbalanced divergence. In order to attain these contributions, a potential vorticity inversion is performed at different stages of the barotropic wave evolution to obtain the balanced and unbalanced fields. A reasonable method to utilize is the set of equations introduced by Lynch (1989) in which the fast modes or IGWs are eliminated from the shallow-water equations. This will also verify whether the magnitude of the divergence tendency is sufficient to produce imbalance within the jet structure. Since IGW activity may always be present to some degree along with numerical noise, it is not expected that the first and higher-order derivatives of divergence will vanish, but if they are of significant magnitude, then the flow may contain IGW activity that affects the

evolution of the flow. It may be expected that the generation of imbalance from an initially balanced condition will arise in a situation in which the divergence is evolving rapidly, and where the projection of the divergence tendency is large enough to excite IGWs that may subsequently interact with the flow.

3.1 Local Rossby and Froude numbers

Large-scale atmospheric motions have been noted observationally to satisfy approximately the gradient wind balance equation or to have a small characteristic Ro . These observations led to the development of the balance equations (Charney 1962; Lorenz 1960) that have since been found to be valid in the limit of small Fr and large Ro (McWilliams 1985). However, the jet structure often has characteristic values of the Rossby and Froude numbers not small with respect to unity, which may inhibit the use of the balance equations. A calculation of jet streak strength and structure, which reflects the shear present in these jets, is the ratio of maximum relative vorticity magnitude to f or the local Ro . Haltiner and Williams (1980) found that a value of the local Ro that exceeds 0.50 was significant enough to make the balance equation no longer formally valid. In their numerical study, Van Tuyl and Young (1982) examined the geostrophic adjustment process in a propagating jet streak in which the jet wind maximum was greater than 50 m s^{-1} , and they found, that as the local Ro approached unity, the amplitude of the unbalanced geopotential, streamfunction, and vertical motion increased significantly.

Figures 1 and 2 indicate the evolution of the local Ro and Fr for each of the three simulations as the barotropic wave increases in amplitude and reaches a maximum value for each parameter. For the strong barotropic jet in this study (simulation (c)), the local Ro remains $O(1)$ as the wave increases in amplitude. The maximum local Fr also remains $O(1)$ throughout the entire simulation because the jet speed does not vary greatly with barotropic integration. From the perspective of scale analysis (e.g. McWilliams 1985; Spall and McWilliams 1992; McIntyre and Norton 2000), it is required that either Ro or Fr must be small for nonlinear balance to be valid; however, neither of these conditions are met for the strong jets. For sufficiently high Ro , such as those

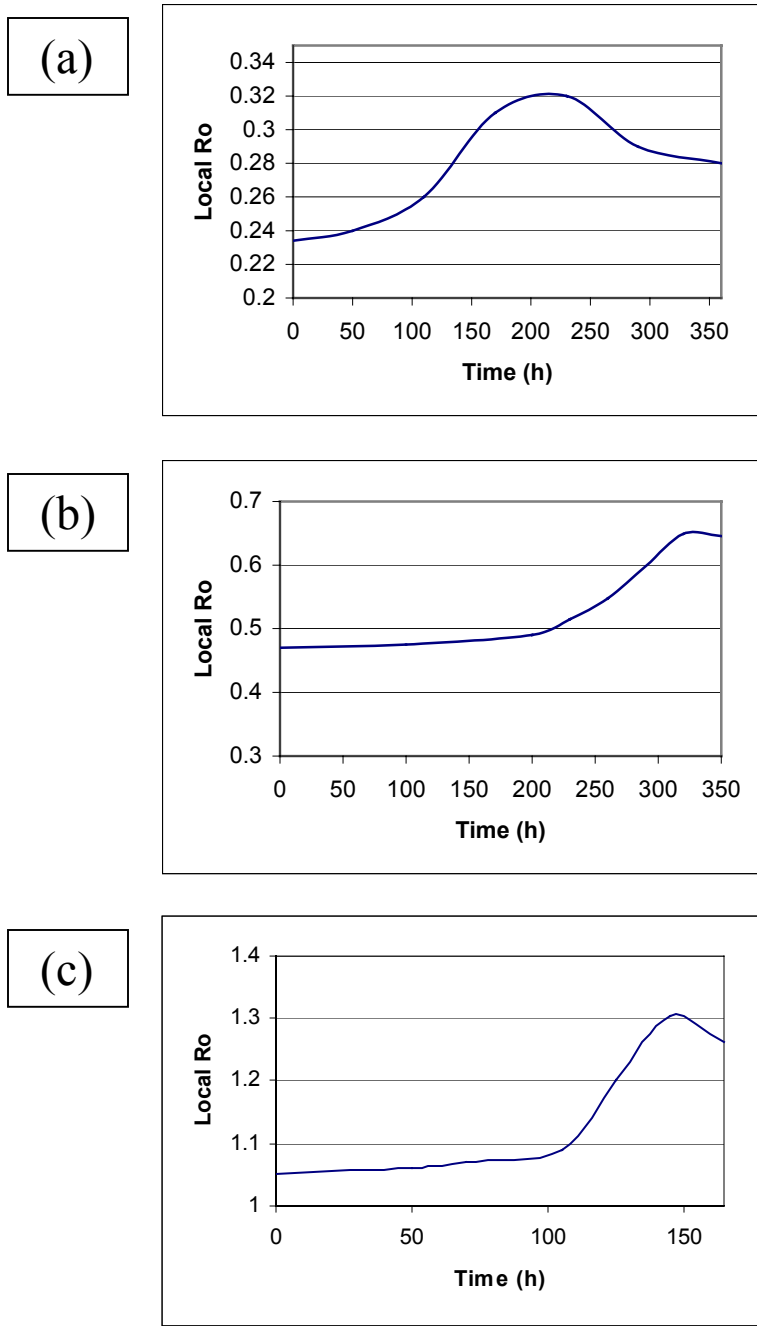


Figure 1: Time series of the local Rossby number for
 (a) $U_o = 20 \text{ m s}^{-1}$, $y_o = 600 \text{ km}$; (b) $U_o = 30 \text{ m s}^{-1}$,
 $y_o = 450 \text{ km}$; (c) $U_o = 60 \text{ m s}^{-1}$, $y_o = 450 \text{ km}$.

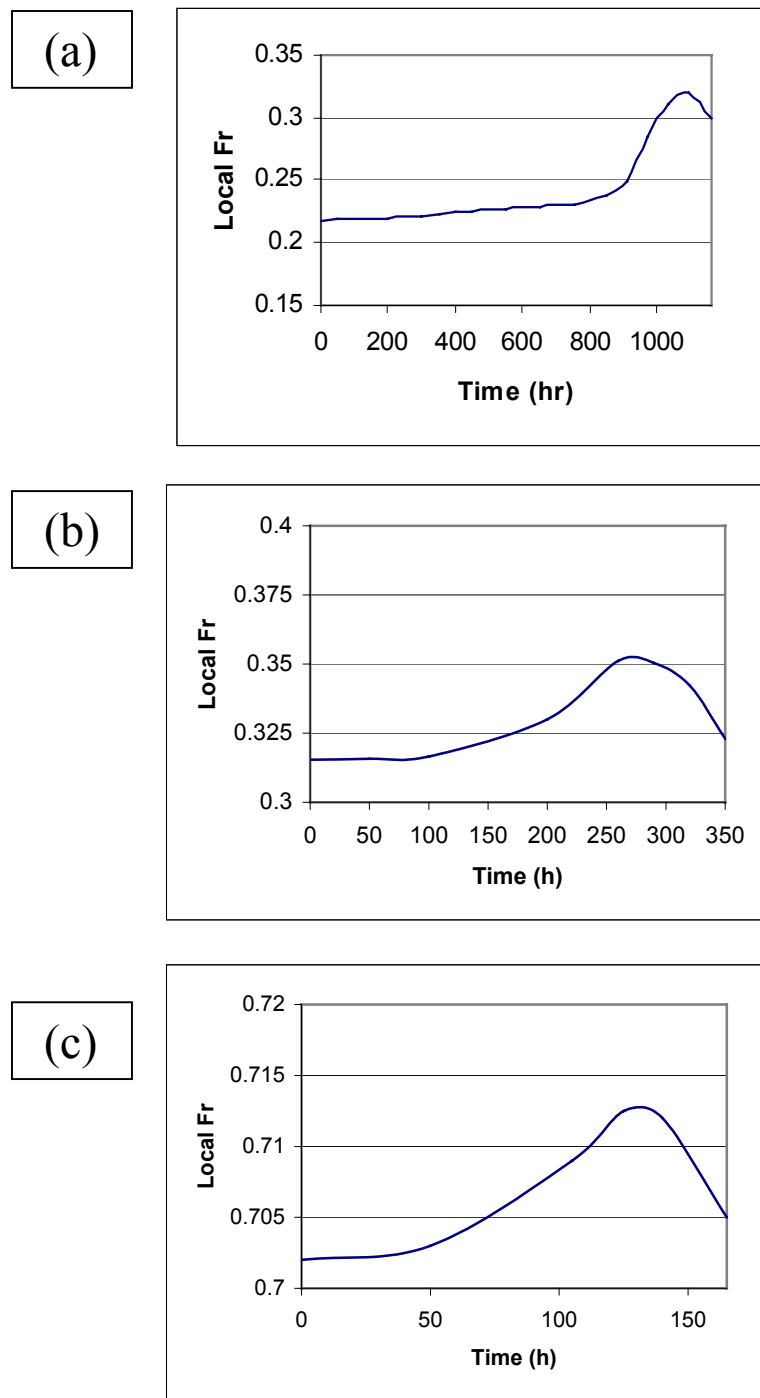


Figure 2: Time series of the local Froude number for
 (a) $U_o = 20 \text{ m s}^{-1}$, $y_o = 600 \text{ km}$; (b) $U_o = 30 \text{ m s}^{-1}$,
 $y_o = 450 \text{ km}$; (c) $U_o = 60 \text{ m s}^{-1}$, $y_o = 450 \text{ km}$.

encountered by jet streaks, secondary motions that are predicted by quasi-geostrophic and Ro or Fr must be small for nonlinear balance to be valid; however, neither of these conditions are met for the strong jets. For sufficiently high Ro , such as those encountered by jet streaks, secondary motions that are predicted by quasi-geostrophic and balance theories would be unable to maintain the balanced condition that exists initially in these simulations and IGWs may result. According to basic scale analysis, a high likelihood of unbalanced flow should occur in the case of the strongest barotropic jet.

3.2 Ratio of divergence to absolute vorticity, δ/ζ and “Gamma parameter”.

Based on ad hoc scale analysis from Haltiner and Williams (1985), the ratio of divergence to relative vorticity is an indicator of the degree of balance present in the growth of an unstable wave. Scaling the shallow-water equations and assuming the wind is nearly geostrophic shows that the ratio of divergence to relative vorticity at any point is on the $O(Ro)$. Small values of this ratio therefore indicate flows in which the balance condition remains valid and can be used to a good approximation of actual flow dynamics. The results show that this ratio remains small for the duration of the simulation for all three cases. For the jet with small Ro_J and Fr_J , the ratio remains $O(10^{-2})$ throughout the entire simulation indicating the balance relation should be a very good approximation to the actual flow. For strong barotropic jets with large Ro_J and Fr_J numbers, it is noted that the ratio remains small, on the $O(10^{-1})$, throughout the entire simulation. Even for the strong barotropic jet, these results indicate that the balance relation would be a good approximation to the actual flow. This contradicts balance studies from other investigators (Spall and McWilliams 1992) where scale analysis of the shallow-water equations predicts the balance relation should breakdown for both large Ro and Fr number.

The evolution of the parameter, γ , for the strong jets (Fig. 3) remain less than $O(10^{-1})$ for the duration of the simulation, such that the maximum horizontal divergence remains small in comparison to the maximum relative vorticity in the entire domain. This also implies that nonlinear balance should remain valid to a good approximation throughout the entire simulation, despite the fact that neither Ro nor Fr is small enough to suggest a

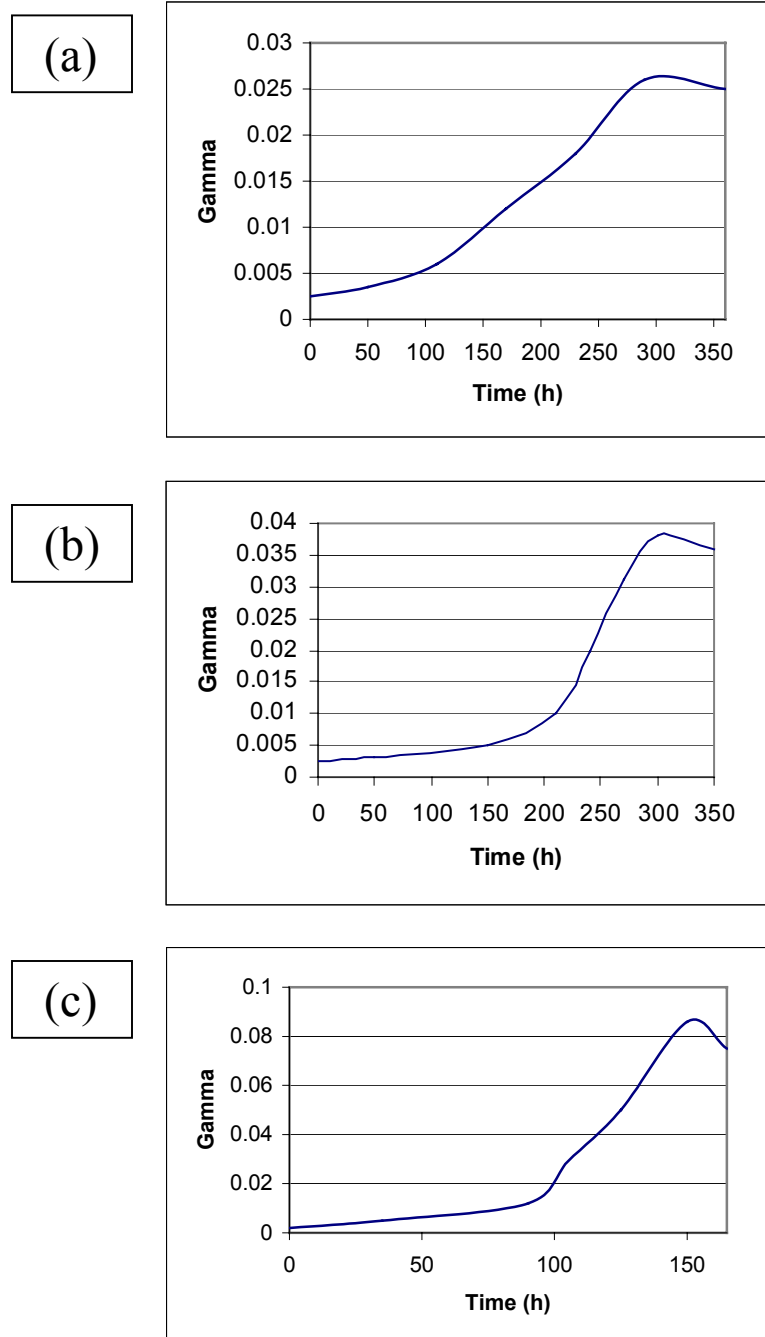


Figure 3: Ratio of maximum horizontal divergence to maximum relative vorticity for (a) $U_o = 20 \text{ m s}^{-1}$, $y_o = 600 \text{ km}$; (b) $U_o = 30 \text{ m s}^{-1}$, $y_o = 450 \text{ km}$; (c) $U_o = 60 \text{ m s}^{-1}$, $y_o = 450 \text{ km}$.

priori that this should be the case. This parameter, as discussed in the Introduction, can also be used as an ad hoc calculation. The results of this parameter are very similar to the results of calculating the ratio at each and every point in the domain, and can be easily utilized as a substitute.

3.3 Lagrangian Rossby number, Ro_L

The Lagrangian Rossby number, Ro_L , is a well known balance indicator and has been utilized by several investigators (e.g. Koch and Dorian 1988, O’Sullivan and Dunkerton 1995,etc.). For each simulation, the Ro_L is calculated at several points in the simulation to indicate its time evolution. IGW generation has been shown, numerically and operationally in baroclinic wave life cycles, to occur when the ratio of the ageostrophic wind to the total wind exceeds 0.5 in an unbalanced flow region (e.g., Van Tuyl and Young 1982). In the simulations shown here, it is found that Ro_L remains small throughout the entire integration of the weak barotropic jet, remaining below a value of 0.1. For the strong barotropic jet, the Ro_L approaches a value ~ 0.3 , but never exceeds 0.5. The maximum value of Ro_L for each simulation is summarized in Table III at the end of the chapter.

However, the largest values of Ro_L occur downstream from the jet core, which is consistent with the greatest values of ageostrophic wind or vertical velocity. The Ro_L values for the strong jet do not exceed the criterion in which unbalanced motions tend to be produced in previous studies, but are coincident with the region of largest imbalance downstream from the jet core (to be shown in the PV inversion section). Investigators have stressed that the Ro_L is an *approximate* indicator and by no means an exact indication of the presence of unbalanced flow and IGWs. Koch and Dorian (1988) presented a more accurate approximation of Ro_L using the cross-stream ageostrophic flow directed toward the cyclonic side of the jet to assess unbalanced flow in the jet exit region (Eq. (19b) in §2.4). They state that this component alone indicates that air parcels are accelerating when they should be decelerating to convert their excess kinetic energy to potential energy. They found that values of this refined estimate of the Ro_L also

exceed 0.5 in the region where $\mathbf{V} > 10 \text{ m s}^{-1}$ particularly at and downstream from the jet core. Even though the calculations of the estimate are not provided here, it is safe to assume that since the value of Ro_L using the total ageostrophic wind is less than 0.5, this refined estimate will even be smaller.

3.4 Divergence and divergence tendency

In a fluid governed by the primitive equations, both low-frequency rotational modes and high-frequency rotational IGWs are possible and may coexist. The latter are commonly associated with significant magnitudes of the horizontal divergence and its time derivatives. Therefore, a dynamical balance that is characterized by the relative unimportance of IGW motions for the evolution of the flow is closely related to the magnitudes of the first and higher-order derivatives of divergence. Interestingly, Shapiro and Montgomery (1993) constructed a balance system in which divergence is not necessarily small for rapidly rotating vortices. Hence, inferring imbalance on the basis of large horizontal divergence may be flawed, requiring that time derivatives of divergence should also be taken into account. For example, in a simulation in which PV is involving rapidly, the divergence field may also evolve rapidly, resulting in a large divergence tendency. What is not clear; however, is whether the divergence tendency can be described as balanced or unbalanced. This observation suggest that although IGW wave activity may arise, it will be weak in some sense, and thus rapid evolution does not necessarily imply imbalance. In this respect, a large divergence tendency may be thought as a necessary, but not sufficient condition for imbalance.

It has been noted that a small material derivative of horizontal divergence typically less than or equal to 10^{-9} s^{-2} has been found to satisfy the nonlinear balance equation. A recent study by O'Sullivan and Dunkerton (1995) yielded numerical simulations in which gravity waves were excited within the numerical simulation of a midlatitude baroclinic wave. They were able to resolve complex patterns of horizontal divergence and divergence tendency that are typical of IGWs. However, they found that the propagation of the IGWs required much greater horizontal and vertical resolution. Just recently, Zhang (2004) basically confirmed O'Sullivan and Dunkerton's results. In the baroclinic wave life cycles, analysis of horizontal divergence indicated gravity wave

activity associated with the surface fronts and cross-frontal ageostrophic circulations. Packets of positive and negative values of horizontal divergence developed within the simulation as the baroclinic wave grew to some finite amplitude. They also found (in agreement with Van Tuyl and Young (1982)) that the upper-level IGWs tend to be confined to the vicinity of the jet stream. The IGWs propagated with wavevector parallel to the jet axis at midstream but at an angle to the jet along its flanks. Both the calculations of the divergence and divergence tendency tended to mimic one another with similar structures, suggesting a wavelike nature.

As will be shown below, the barotropic model simulations, the divergence patterns associated with the wave amplitude for large Ro and Fr never show the type of structure associated with IGWs found in a baroclinic model. The divergence fields remain smooth, indicating positive and negative centers increasing with magnitude, but with no smaller scale structure. The divergence tendency fields associated with the barotropic waves also do not exhibit the smaller scale structure found in numerical simulations of IGWs, even at very high resolution. In fact, the model calculated divergence tendency for all the simulations shown here remains on the $O(10^{-10})$ throughout the simulation, even for the case of large Rossby and Froude numbers. Nevertheless, this calculation provides evidence of the possible lack of imbalance in all the simulations and is summarized at the end of the chapter in Table III.

3.5 Basic jet evolution and PV inversion

The evolution of several parameters including the total wind, divergence, relative vorticity, and potential vorticity of each simulation is presented in the following figures:

- (a) $U_o = 20 \text{ m s}^{-1}$, $y_o = 600 \text{ km}$; Figs. 4-7
- (b) $U_o = 30 \text{ m s}^{-1}$, $y_o = 450 \text{ km}$; Figs. 12-15
- (c) $U_o = 60 \text{ m s}^{-1}$, $y_o = 450 \text{ km}$; Figs. 20-23.

The simulations begin with an initially balanced jet, and are allowed to grow with the addition of a perturbation. This jet continues to grow in amplitude over time to produce dynamical fields consistent with barotropic instability. Each simulation also conserves known domain invariants, such as energy and potential enstrophy, to a very high degree. The figures represent the time in each simulation in which the fields begin to develop

structure (v -component of the wind is becomes greater than 1 m s^{-1}). These fields, such as the total divergence field, are shown to compare with the balanced and unbalanced divergence fields calculated from the PV inversion (below). The relative vorticity and PV fields are shown to further indicate the growth of the wave instability and indicate their structure in relation to the other fields. All three simulations are presented at times in which the wave amplitude and dynamical fields are similar in structure for easy contrasts and comparison, especially with regards to the PV inversion.

The bulk of this thesis and most significant portion of this study involve the use of PV inversion to recover the balanced and unbalanced motions from each of the simulations. The PV is a remarkable property attributed to fluid motion as shown by Rossby (1936) in which the PV is an exact material invariant of inviscid stratified, rotating flow. The idea is recognized in modern fluid dynamics as being central to understanding the dynamical behavior of the atmosphere. As for the concept of balanced flow, the “invertibility principle” of PV is a pioneering concept introduced in a landmark paper by Hoskins, et al. (1985). As discussed previously, the invertibility principle states that if the total mass under each isentropic surface is specified, then a knowledge of the global distribution of PV is sufficient, at some given instant, to implicitly contain all the remaining dynamical information about the flow at that instant. In other words, balance and invertibility mean that not only sound waves but also freely-propagating IGWs contribute only negligibly to the full fluid motion. Invertibility, however, depends on the precise balance assumption used in the model. For example, in a nondivergent, barotropic fluid, the balanced flow and actual flow are identical. However, the balanced flow is only an approximation to the total flow in the real atmosphere. The accuracy of this approximation depends on the validity of the scaling assumptions used to define the invertibility problem. From the PV perspective, scientists have gained knowledge, appreciation, and a better understanding of classical synoptic phenomena, as well as IGW development from atmospheric unbalance.

The PV inversion method utilized in this study is derived from Lynch (1989) as discussed in Chapter 2. By eliminating the time tendencies of divergence and geostrophic imbalance from the shallow-water equations, the fast modes, or IGW solutions, are eliminated, leaving only the balanced fields. Lynch refers to this system of equations as

the “slow equations”. For clarification, the geostrophic imbalance tendency from the combination of the vorticity and continuity equations and the divergence tendency from the divergence equation are eliminated which filters out these high frequency or IGW modes. The equation for the tendency of geostrophic imbalance is (29) in §2.5:

$$\dot{\varepsilon} + \left(\nabla^2 - f_o^2 / \bar{\Phi} \right) \bar{\Phi} \delta = - \left(\nabla^2 N_\Phi - f_o N_\zeta \right) \quad (45)$$

where

$$\dot{\varepsilon} = \frac{d}{dt} \left(\nabla^2 \Phi - f_o \zeta \right). \quad (46)$$

The equation for geostrophic balance is simply,

$$\nabla^2 \Phi = f_o \zeta, \quad (47)$$

which is obtained from elimination of the small nonlinear terms and the divergence tendency in the divergence equation. Elimination of these terms stems from their extremely small magnitude in flows that are characterized as geostrophic. Geostrophic imbalance, on the other hand, is simply the difference of the two terms in (47), and a large difference indicates the nonlinear terms in the divergence equation are not negligible and geostrophic balance is no longer valid. It has been shown, the fast modes project onto the time tendency of divergence and geostrophic imbalance and the PV inversion indicates the contribution of these terms to the total flow.

The unbalanced fields in the PV inversion are found by simply subtracting the balanced fields from the fields given by the full integration of the shallow-water equations. After integration of each simulation to some finite amplitude, the geopotential height and horizontal wind data are sent to the Helmholtz solvers to obtain the balanced and unbalanced fields as discussed in Chapter 2. The balanced and unbalanced fields are then plotted and examined for each of the simulations. Again, the difference between the initial and balanced fields elucidates unbalanced features that may indicate a region of unbalanced flow and possible IGW formation that may result from this imbalance.

A. $U_o = 20 \text{ m s}^{-1}$ and $y_o = 600 \text{ km}$

Figs. 8 - 11 show the evolution of the balanced and unbalanced geopotential and divergence fields for the low Rossby and Froude number simulation. A low Ro and Fr

number indicates a flow which should be balanced to a very high degree due to a very small growth rate (i.e. slow evolution; $O(10^{-6})$), and dynamic fields, such as the divergence, evolving without rapid changes. Scale analysis of the shallow-water equations readily shows flows with low Ro and Fr numbers basically can be described by nonlinear balance. The results of the PV inversion for the unbalanced geopotential and divergence remain extremely small compared to the total geopotential and divergence fields throughout the entire simulation. Maximum values of the unbalanced geopotential remain on the $O(10^{-4})$ compared to the total geopotential field and the subsequent unbalanced divergence values remain on the $O(10^{-2})$ compared to the total divergence field. The PV inversion agrees with the previous analyses that the simulation virtually remains very balanced throughout its life cycle.

B. $U_o = 30 \text{ m s}^{-1}$ and $y_o = 450 \text{ km}$

The intermediate Rossby and Froude number simulation in Figs. 16 – 19 show the evolution of the balanced and unbalanced fields. The jet Rossby number for this case (0.7) is now approaching $O(1)$ while the jet Froude number (0.3) remains less than unity. As discussed previously, as the Ro and Fr numbers increase, the flow is less likely to remain in a balanced state and therefore unbalanced motions should begin to develop as the wave amplitude grows. The evolution of the unbalanced geopotential for this case; however, remains small compared to the total geopotential ($O(10^{-3})$), and the unbalanced divergence is only of the $O(10^{-1})$ compared to the total divergence throughout the simulation. The difference in this simulation compared with the low Ro and Fr number case is that an unbalanced divergence field structure readily grows as the wave amplitude increases. In Figs. 18 and 19, the maximum unbalanced divergence, albeit small, occurs downstream from the jet streak as air parcels decelerate rapidly after emerging from the jet streak. Also, this maximum region of unbalanced motion also occurs in the region of highly curved flow between the jet ridge and trough in which parcels suddenly change direction. This region of largest imbalance is consistent with the conceptual model introduced by Uccellini and Koch (1987) indicating the greatest unbalanced flow and subsequent IGW generation should occur in this particular region. However, the magnitude of the unbalanced fields is very small, and IGWs are more than likely not

occurring as the wave amplitude grows. This is substantiated by the fact that the growth rate remains small $O(10^{-6})$, and the PV inversion results agree with the previous diagnostic calculations indicating IGW formation is very unlikely. Therefore, the evolution of the wave is slow enough in order for the wave to remain essentially balanced throughout its life cycle.

C. $U_o = 60 \text{ m s}^{-1}$ and $y_o = 450 \text{ km}$

The large Rossby and Froude number case (Figs. 24 – 27), in theory, should contain significant unbalanced motions that subsequently lead to IGW formation. Scale analysis (McWilliams 1985; Spall and McWilliams 1992) indicates that flows with large Ro and Fr number should invalidate the balance condition imposed and imbalance should result. The values of unbalanced geopotential and divergence fields are larger in comparison to the previous simulations; however, their magnitude compared to the total fields are small. The unbalanced geopotential remains on the $O(10^{-3})$ compared to the total geopotential, and the unbalanced divergence remains $O(10^{-1})$ compared to the total divergence throughout the entire simulation. The structure of the unbalanced divergence field in Fig. 27 clearly indicates the maximum unbalanced divergence occurs downstream from the jet streak in the region of highly curved flow. Again, the magnitude of the imbalance is very small, and IGW formation is unlikely to occur, even though clear structures of unbalanced divergence are readily apparent. The growth rate, albeit larger than the other two simulations, is of the $O(10^{-5})$ indicating that slow evolution of the wave still prevents large imbalances from developing. Again, this is consistent with the previous analyses and shows that the evolution of a barotropic wave utilizing the shallow-water equations remains balanced to a high degree, even though Rossby and Froude numbers are $O(1)$ in strong jets. The high resolution of the model enables small-scale features in the unbalanced fields to be examined in these simulations, and the resulting balanced winds from the PV inversion indicate very little change from the total wind field. This allows us to conclude that IGWs ultimately are unlikely to develop from an initially balanced barotropic shallow-water equation model. These results, including all the parameters discussed in this chapter, are summarized in Table III.

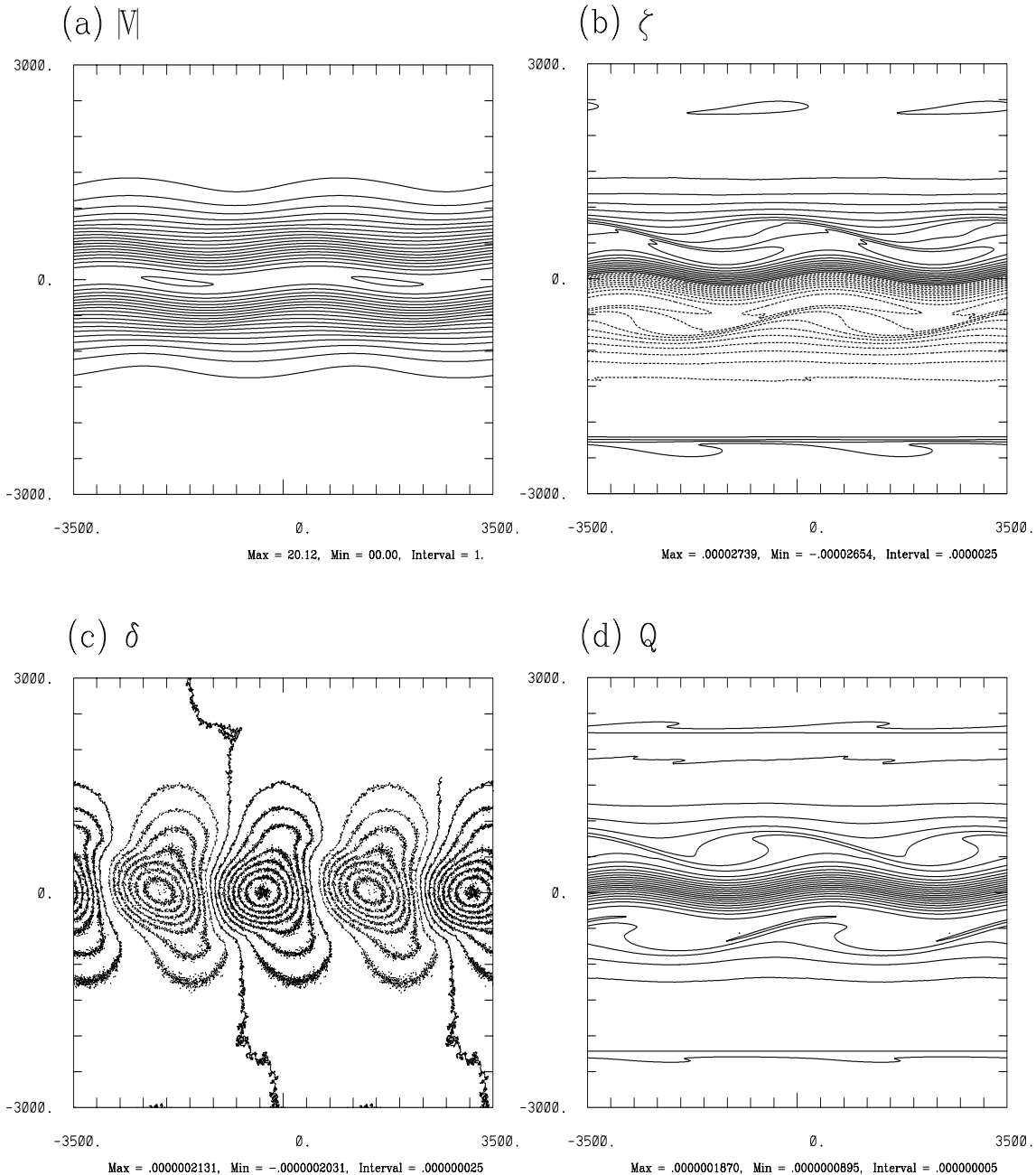


Figure 4: Dynamic fields for $U_o = 30 \text{ m s}^{-1}$ and $y = 600 \text{ km}$ at $t = 180 \text{ h}$ including:

(a) wind speed (m s^{-1}), (b) relative vorticity (s^{-1}), (c) horizontal divergence (s^{-1}), and (d) potential vorticity (s^{-1}). Maximum/minimum values along with contour are indicated.

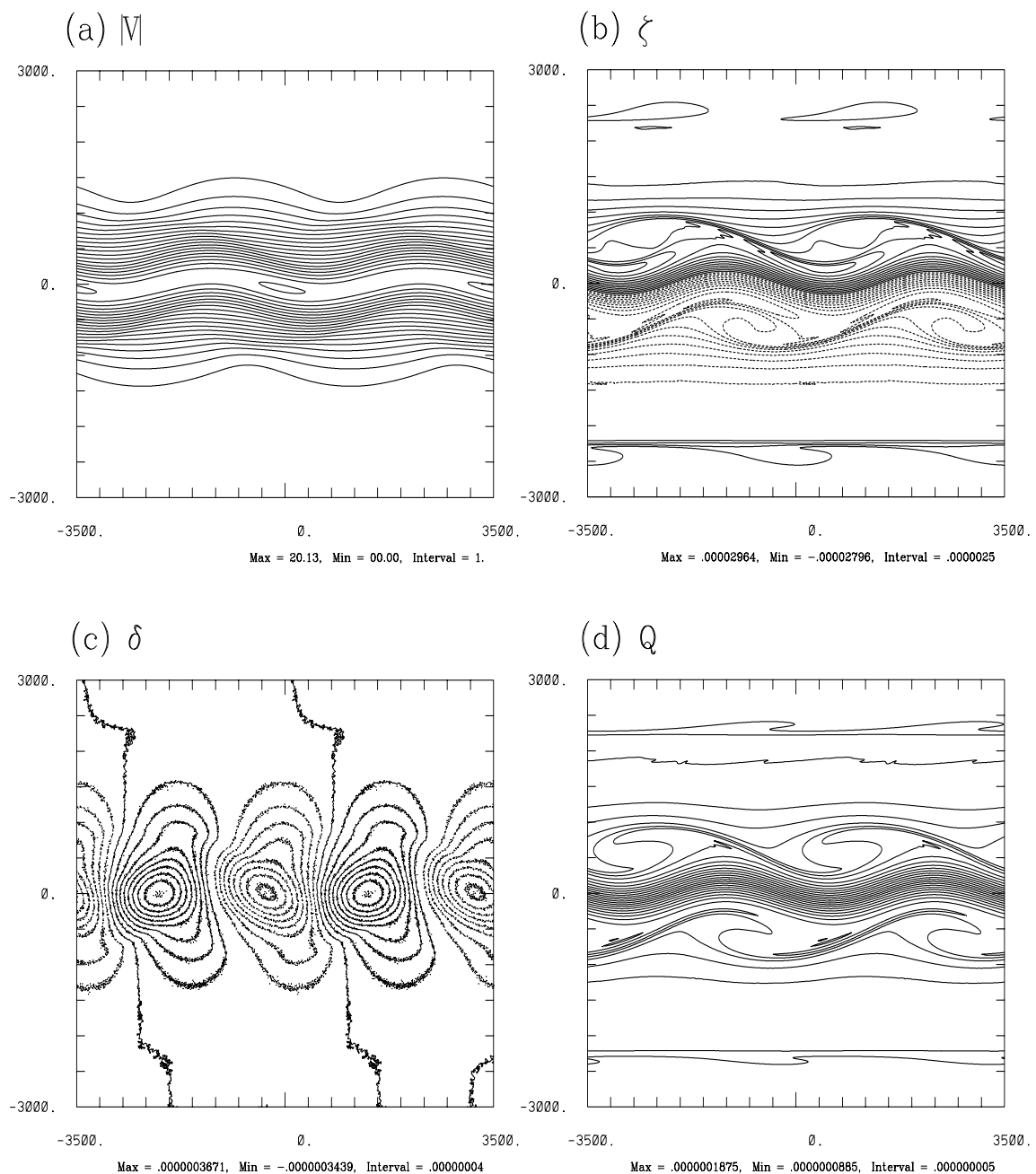


Figure 5: As in Fig. 4 but for $t = 240$ h.

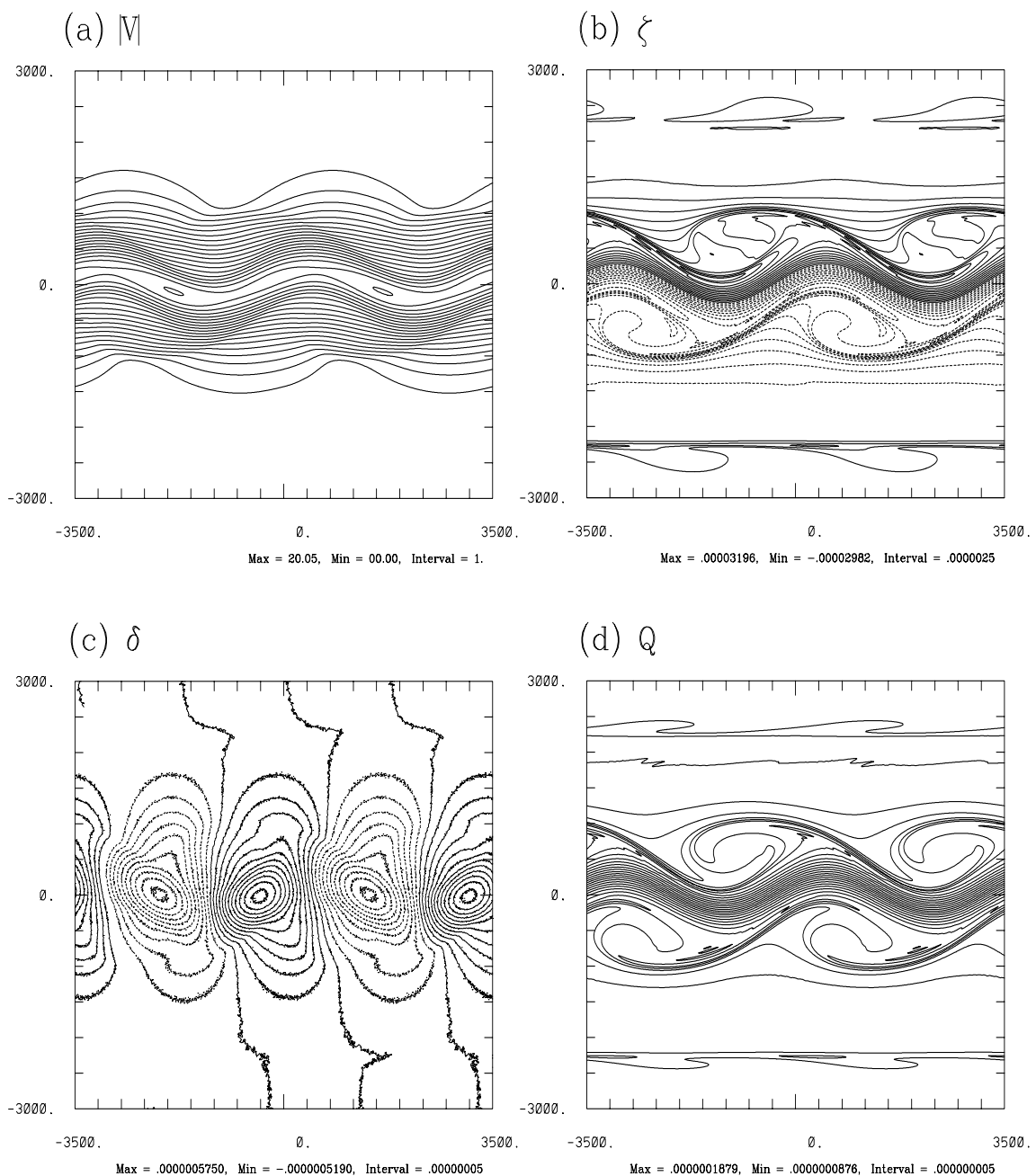


Figure 6: As in Fig. 4 but for $t = 300$ h.

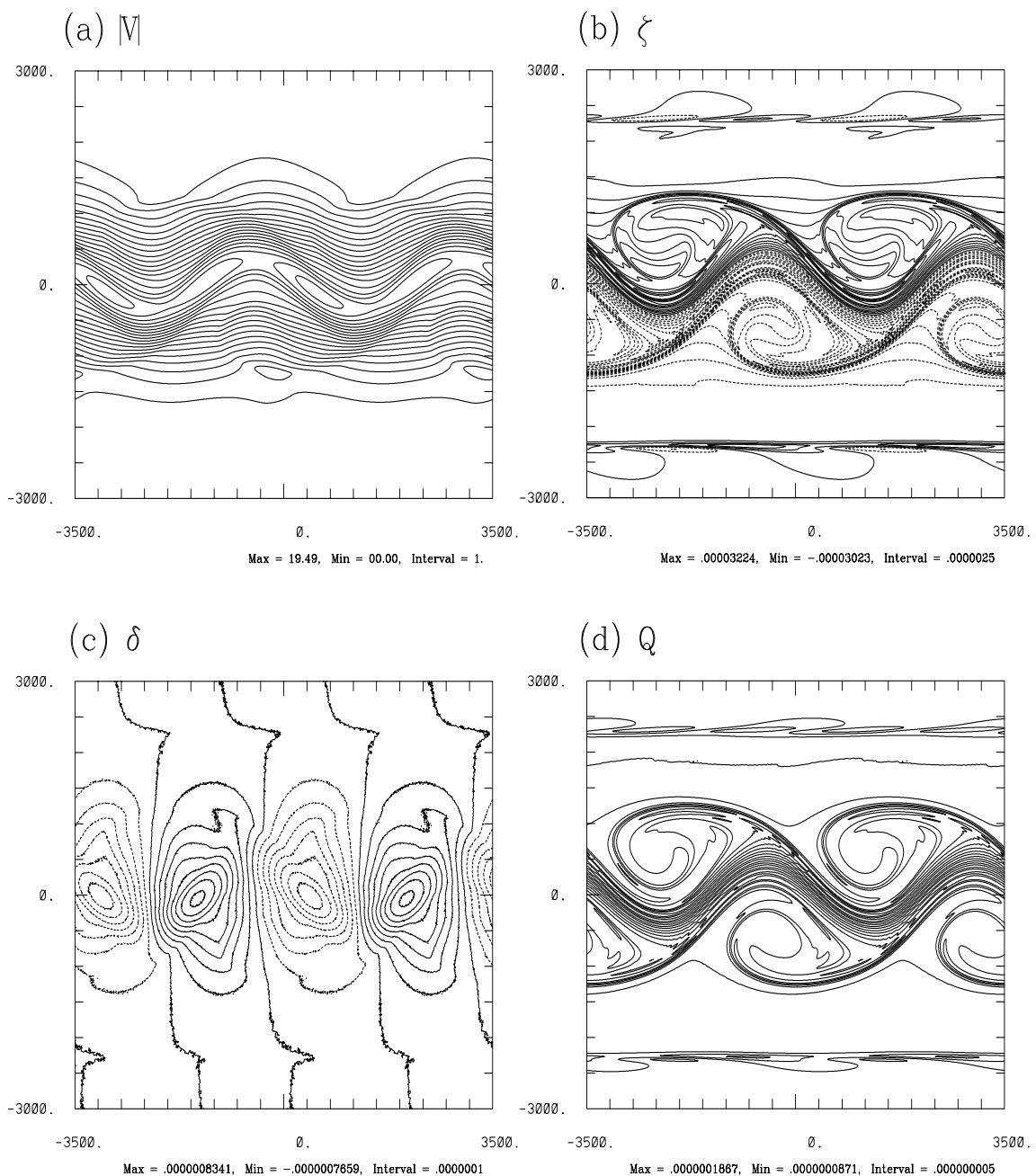
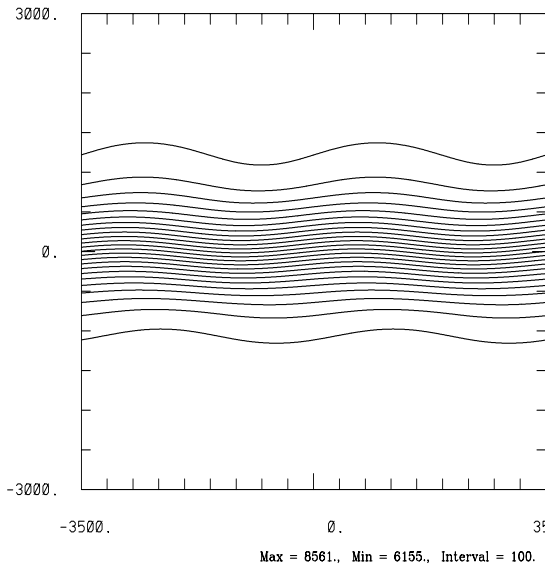
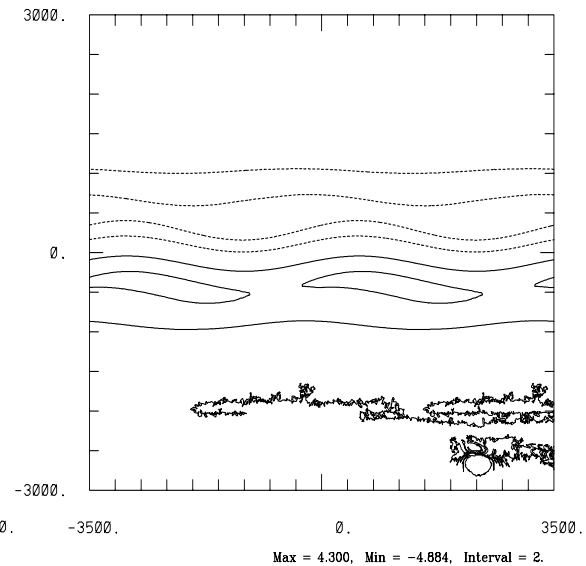


Figure 7: As in Fig. 4 but for $t = 360$ h.

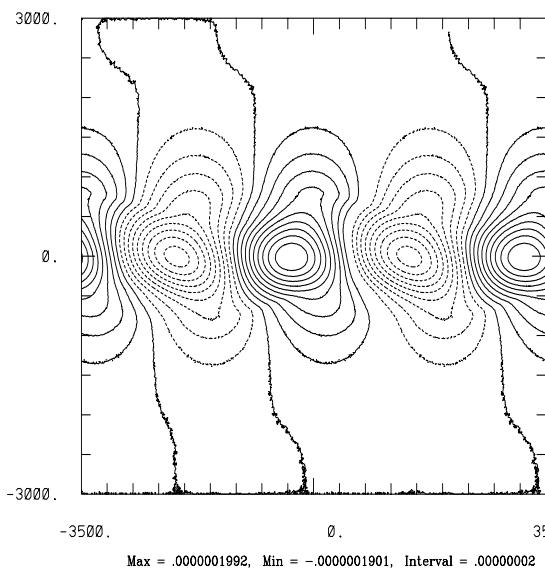
(a) Balanced Φ



(b) Unbalanced Φ



(c) Balanced δ



(d) Unbalanced δ

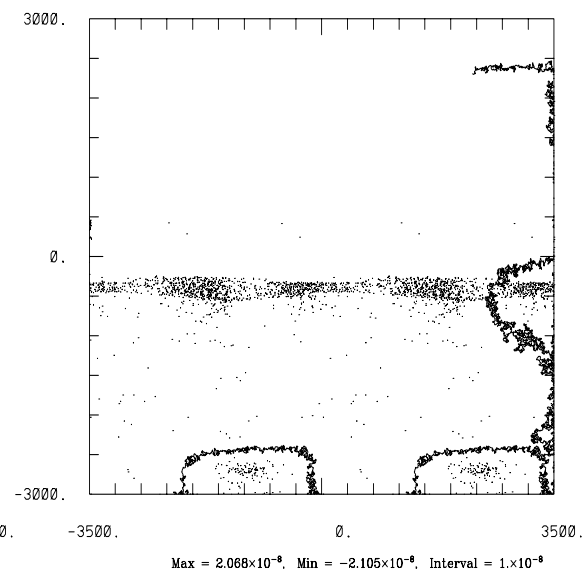
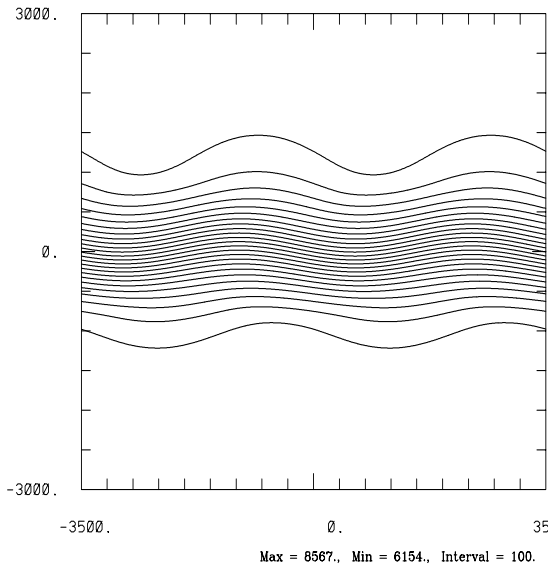
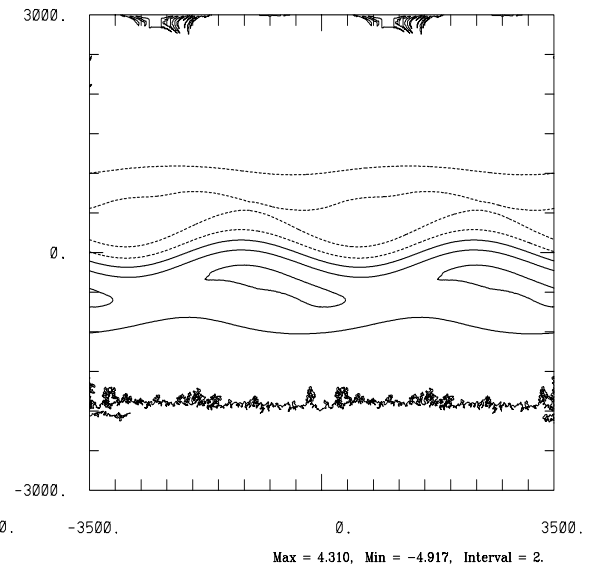


Figure 8: Balanced and unbalanced geopotential height ($m^2 s^{-2}$) and horizontal divergence (s^{-1}) plots for $t = 180$ h.

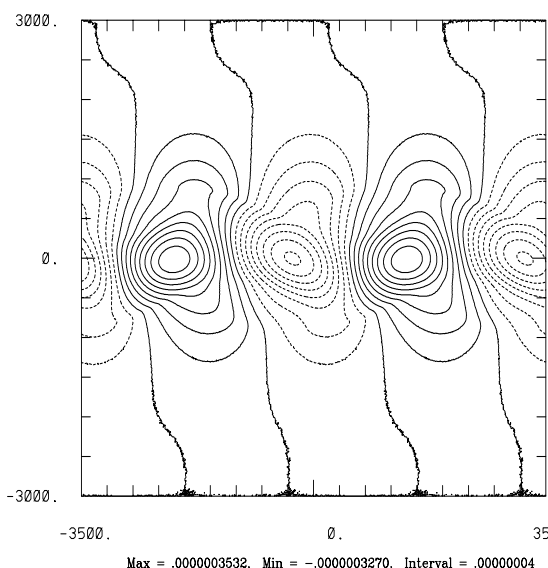
(a) Balanced Φ



(b) Unbalanced Φ



(c) Balanced δ



(d) Unbalanced δ

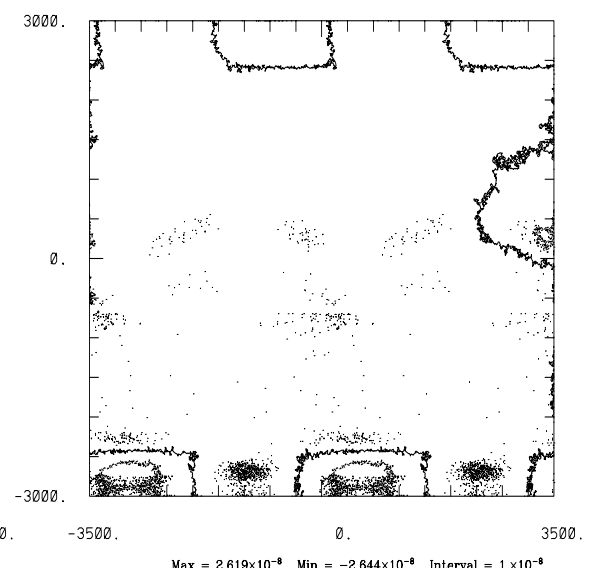
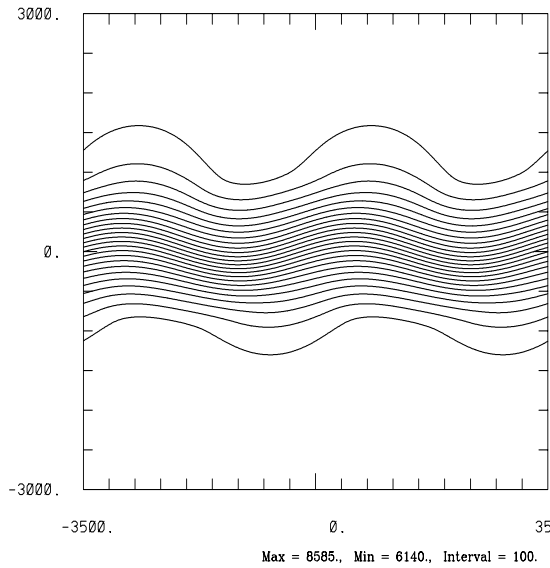
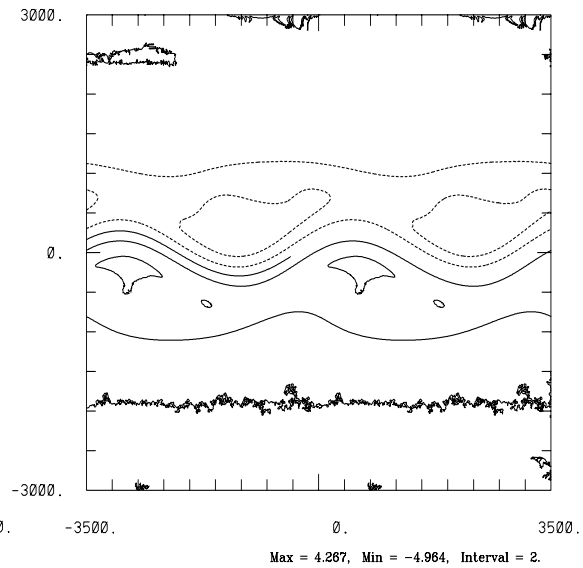


Figure 9: As in Fig. 8 but for $t = 240$ h.

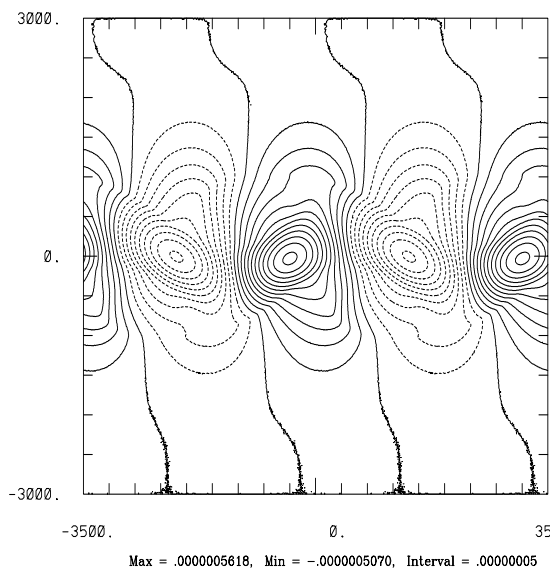
(a) Balanced Φ



(b) Unbalanced Φ



(c) Balanced δ



(d) Unbalanced δ

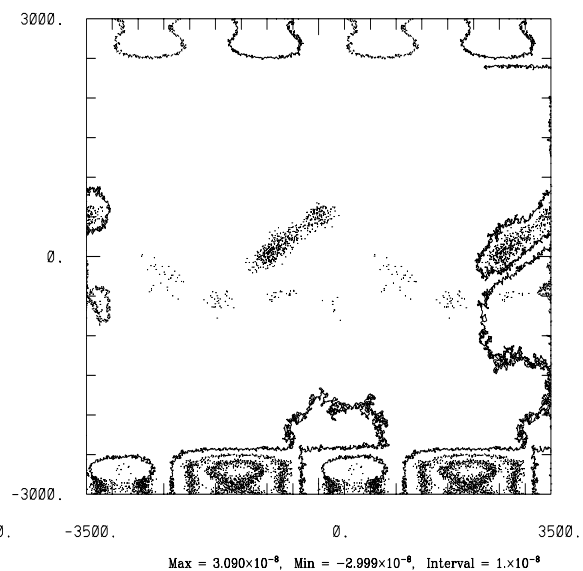
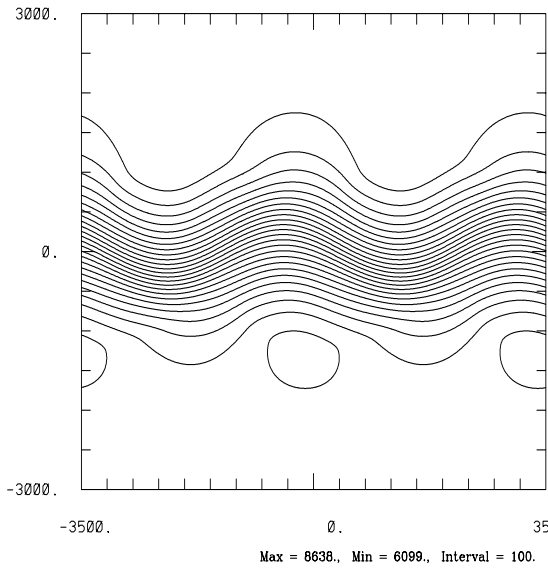
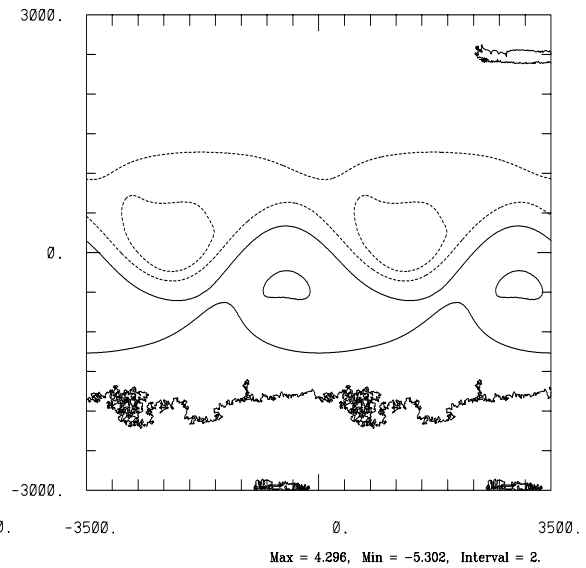


Figure 10: As in Fig. 8 but for $t = 300$ h.

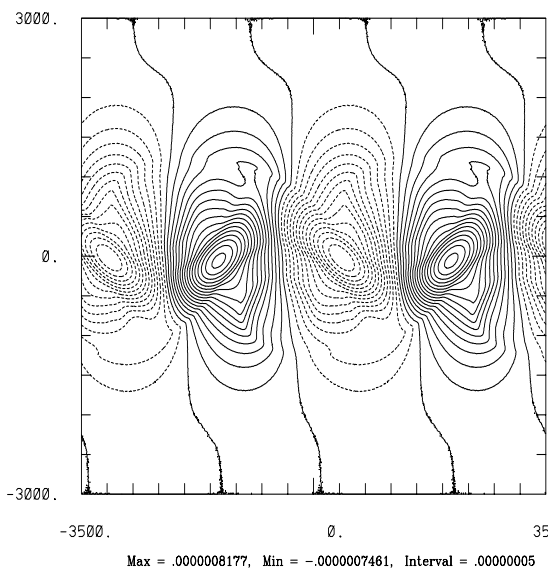
(a) Balanced Φ



(b) Unbalanced Φ



(c) Balanced δ



(d) Unbalanced δ

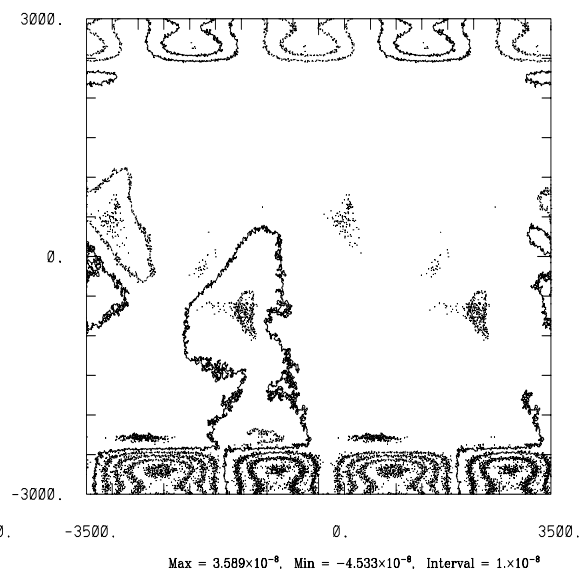


Figure 11: As in Fig. 8 but for $t = 360$ h.

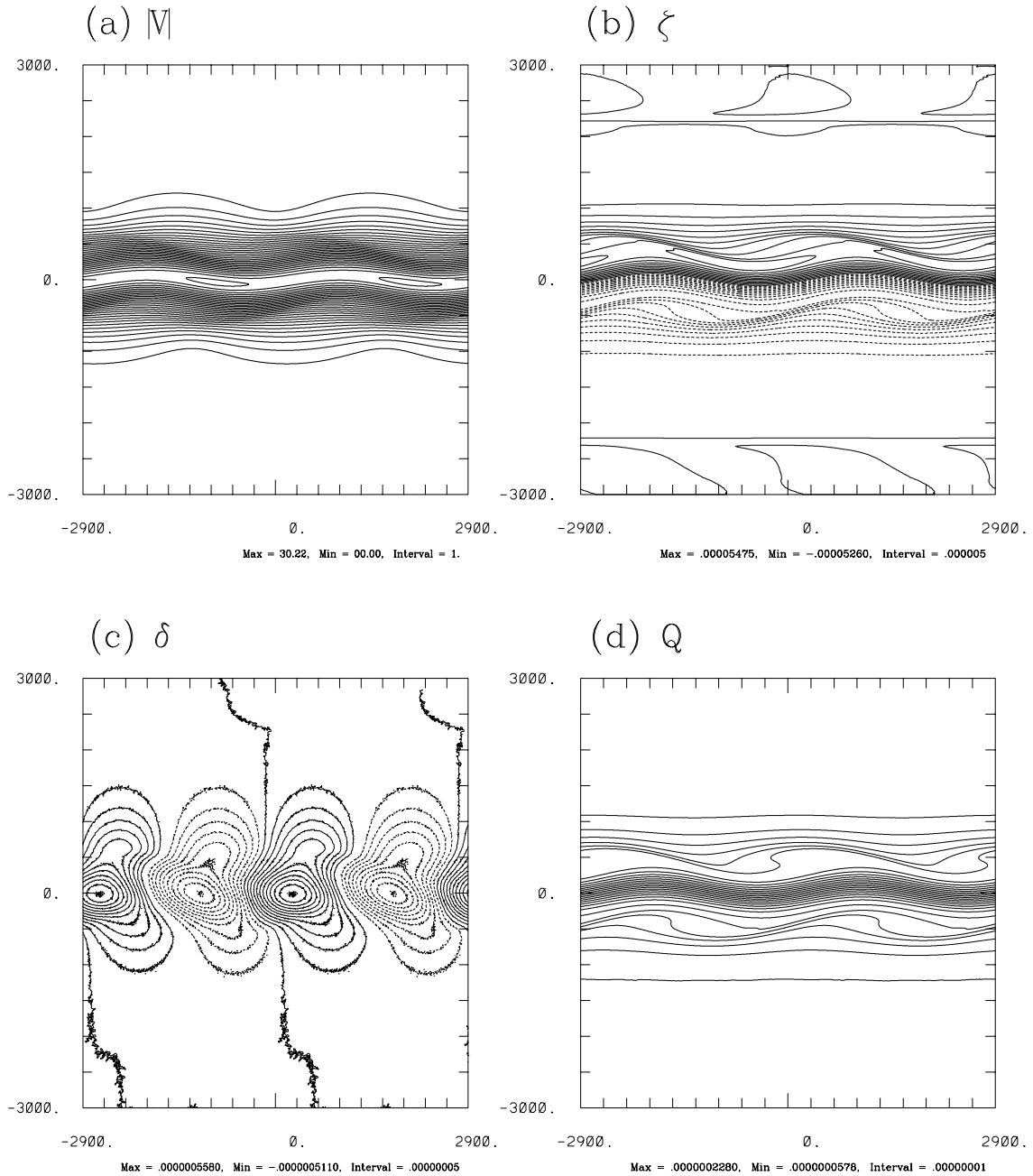


Figure 12: Dynamic fields for $U_0 = 30 \text{ m s}^{-1}$ and $y = 450 \text{ km}$ at $t = 260 \text{ h}$ including:
 (b) wind speed (m s^{-1}), (b) relative vorticity (s^{-1}), (c) horizontal divergence (s^{-1}),
 and (d) potential vorticity (s^{-1}). Maximum/minimum values along with contour
 intervals are indicated.

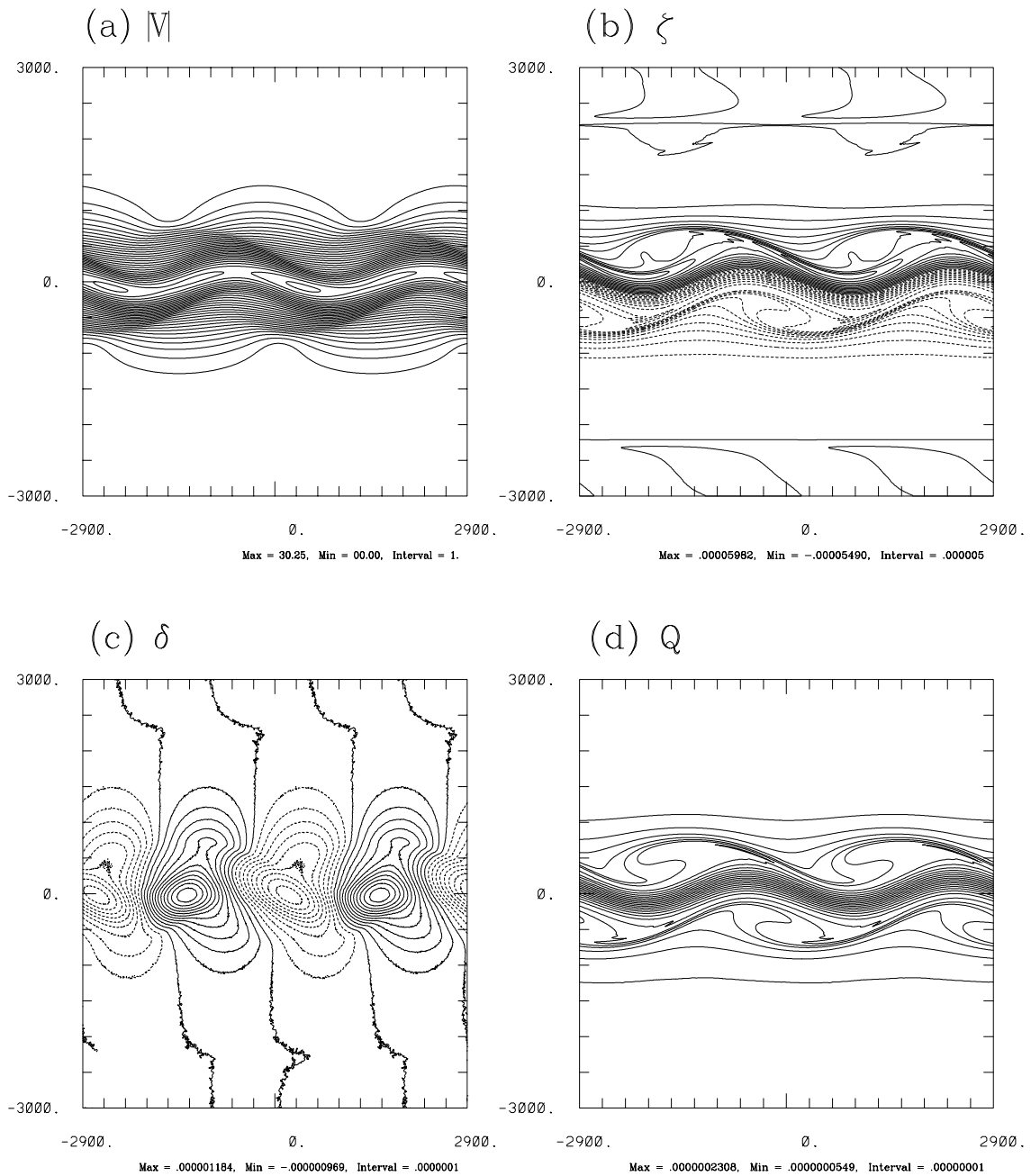


Figure 13: As in Fig. 12 but for $t = 290$ h.

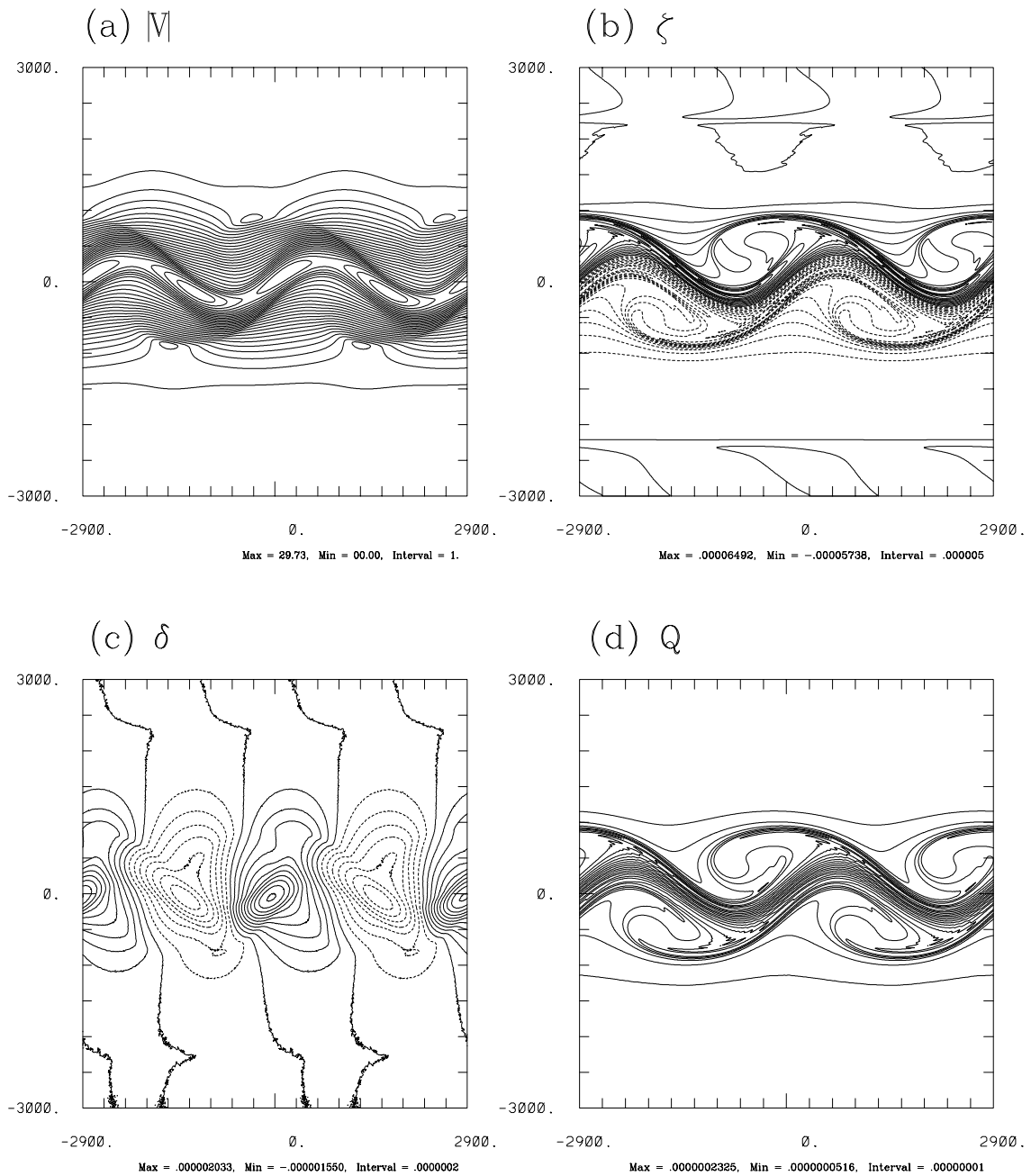


Figure 14: As in Fig. 12 but for $t = 320$ h.

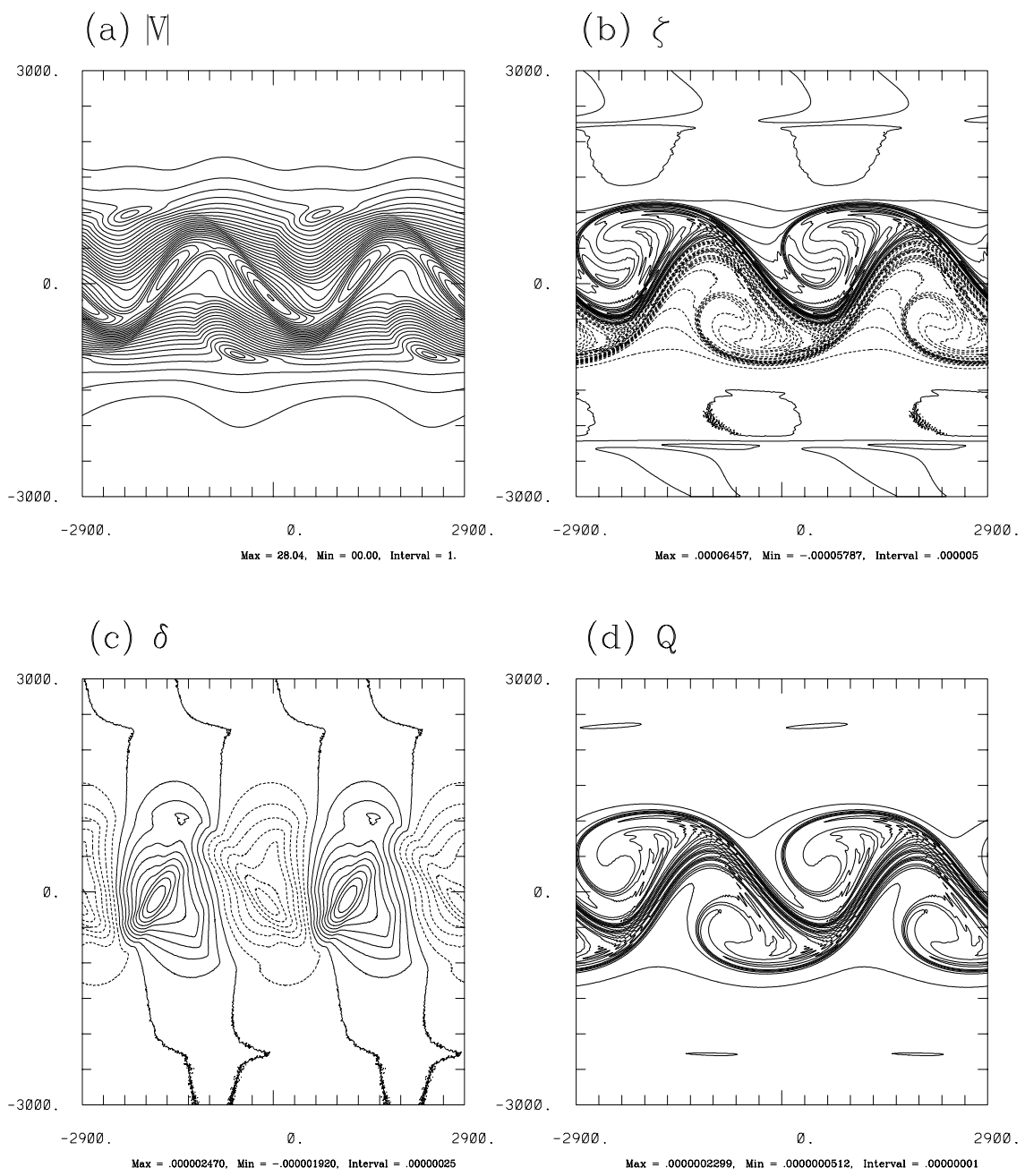
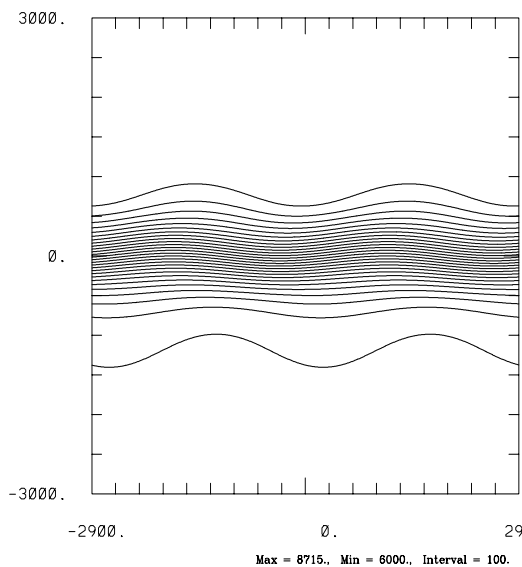
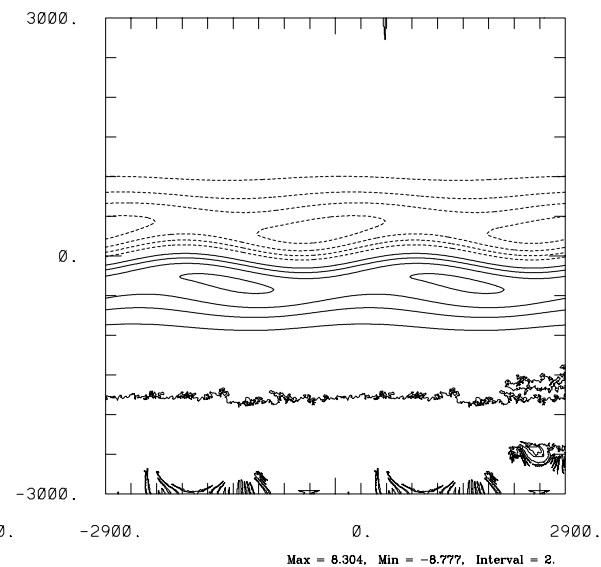


Figure 15: As in Fig. 12 but for $t = 350$ h.

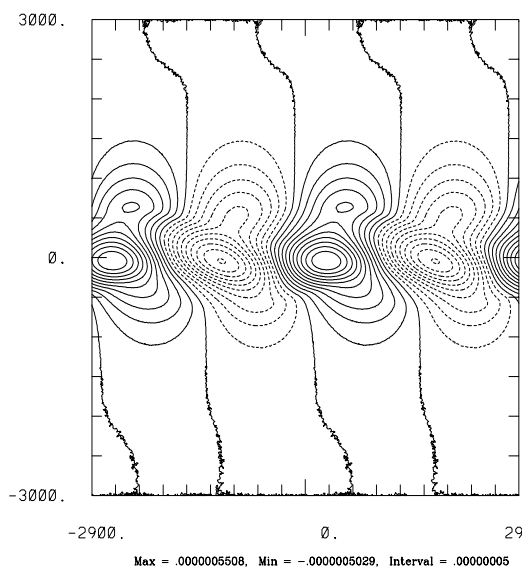
(a) Balanced Φ



(b) Unbalanced Φ



(c) Balanced δ



(d) Unbalanced δ

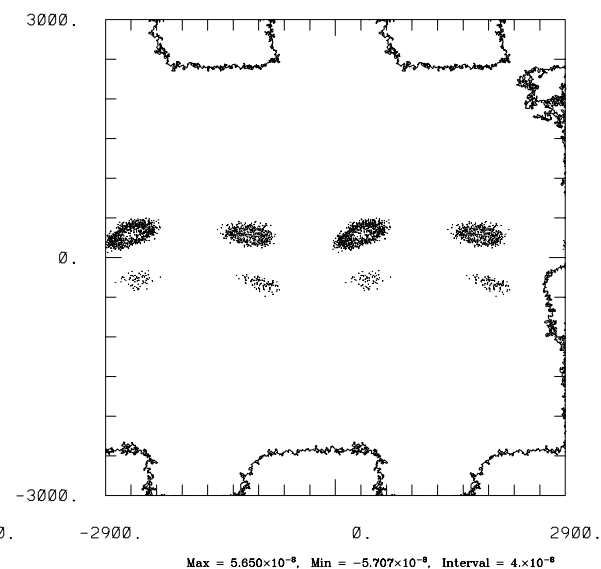
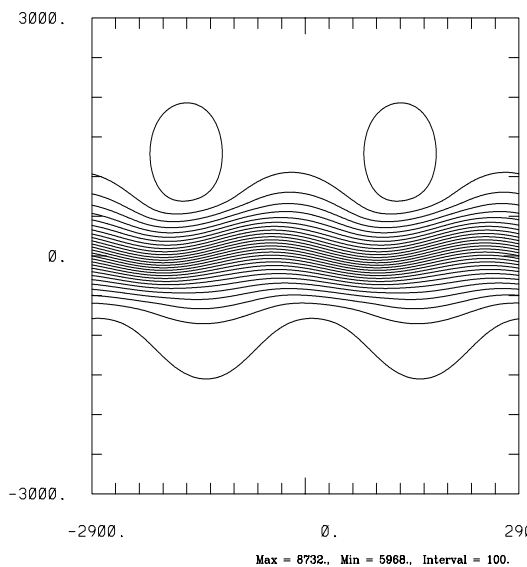
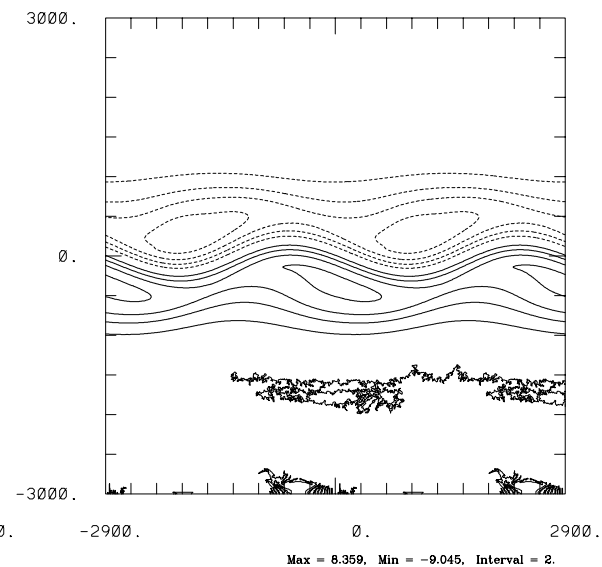


Figure 16: Balanced and unbalanced geopotential height ($\text{m}^2 \text{s}^{-2}$) and horizontal divergence (s^{-1}) plots for $t = 260$ h.

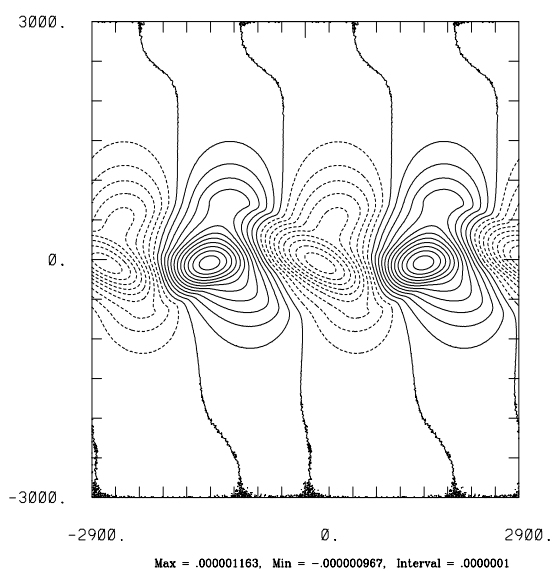
(a) Balanced Φ



(b) Unbalanced Φ



(c) Balanced δ



(d) Unbalanced δ

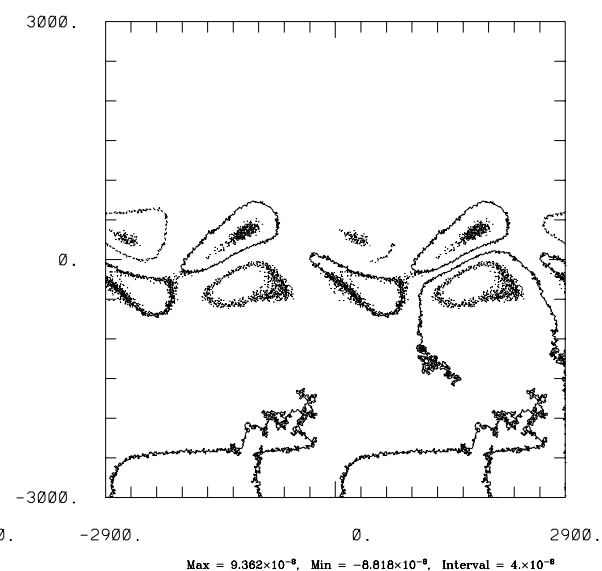
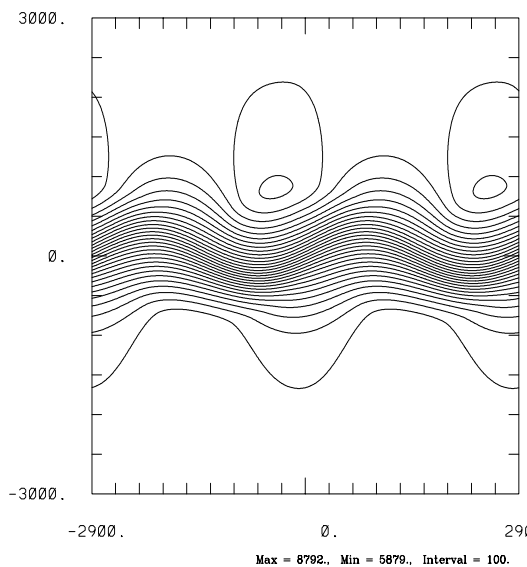
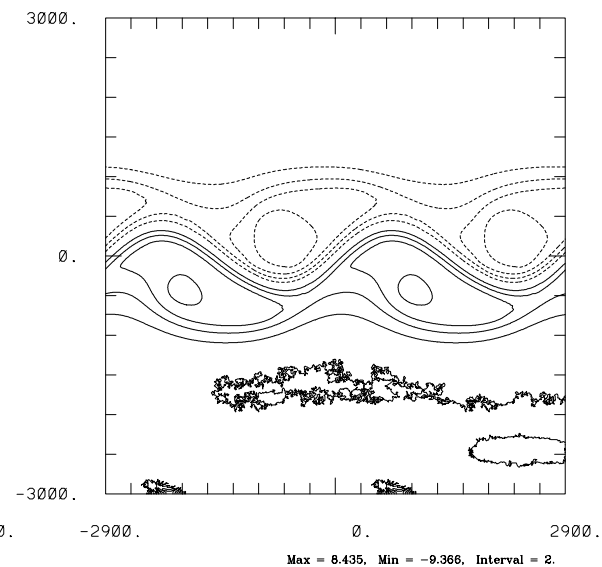


Figure 17: As in Fig. 16 but for $t = 290$ h.

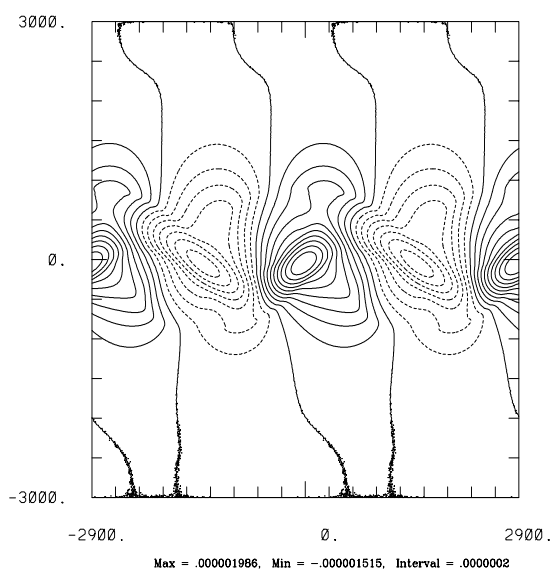
(a) Balanced Φ



(b) Unbalanced Φ



(c) Balanced δ



(d) Unbalanced δ

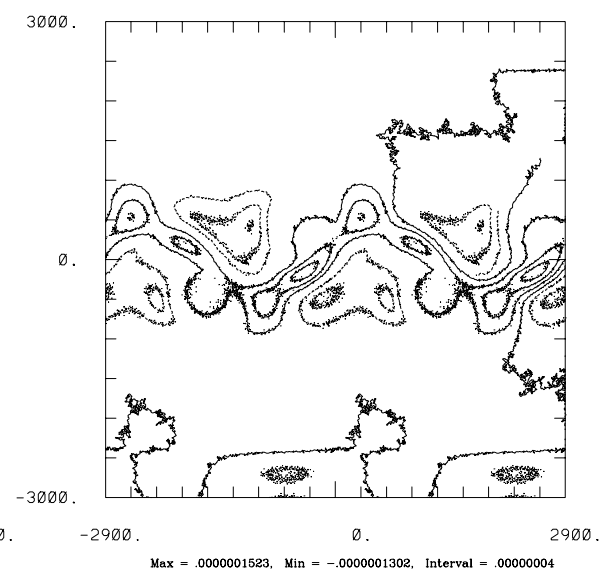
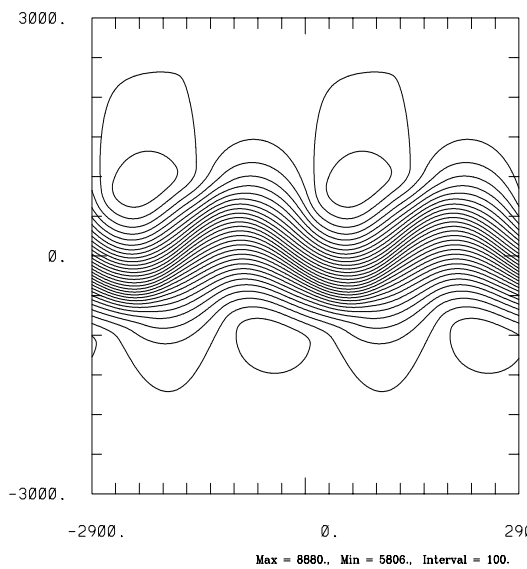
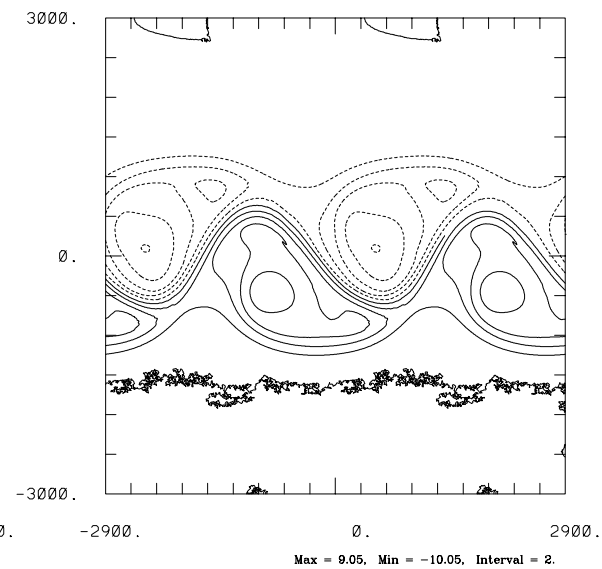


Figure 18: As in Fig. 16 but for $t = 320$ h.

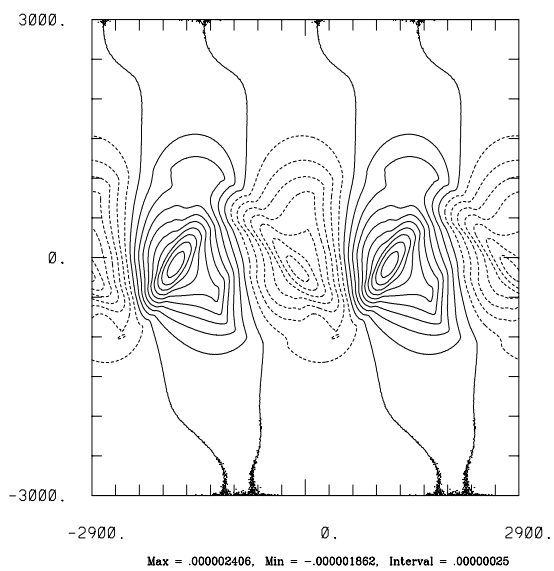
(a) Balanced Φ



(b) Unbalanced Φ



(c) Balanced δ



(d) Unbalanced δ

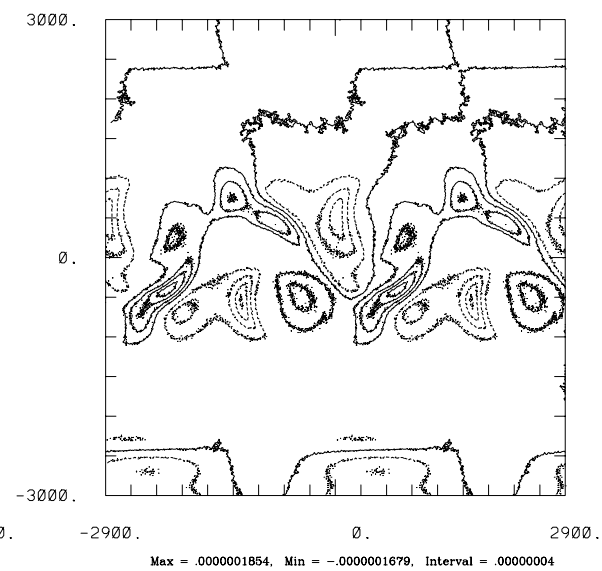


Figure 19: As in Fig. 16 but for $t = 350$ h.

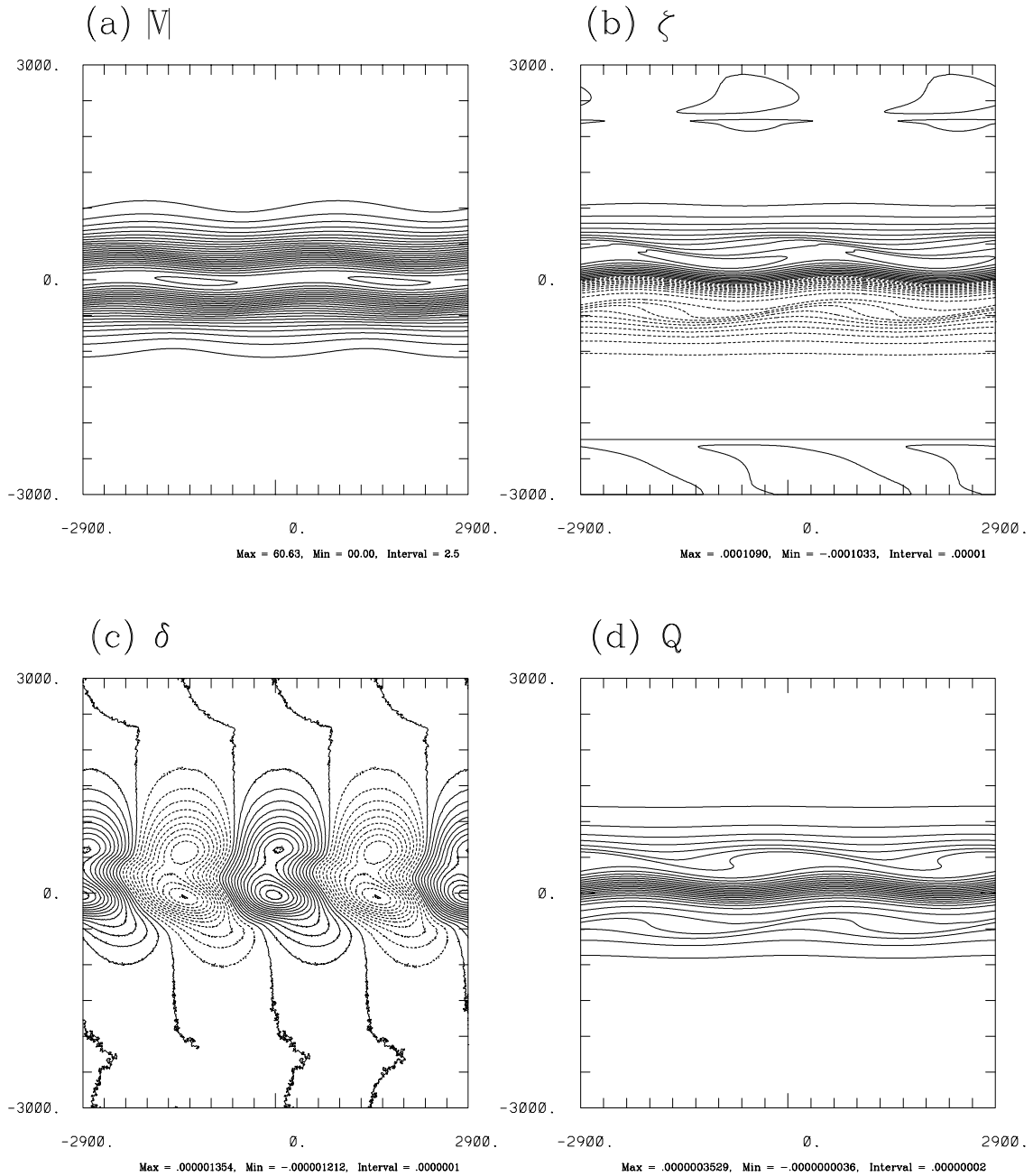


Figure 20: Dynamic fields for $U_0 = 60 \text{ m s}^{-1}$ and $y = 450 \text{ km}$ at $t = 90 \text{ h}$ including:
 (c) wind speed (m s^{-1}), (b) relative vorticity (s^{-1}), (c) horizontal divergence (s^{-1}),
 and (d) potential vorticity (s^{-1}). Maximum/minimum values along with contour
 intervals are indicated.

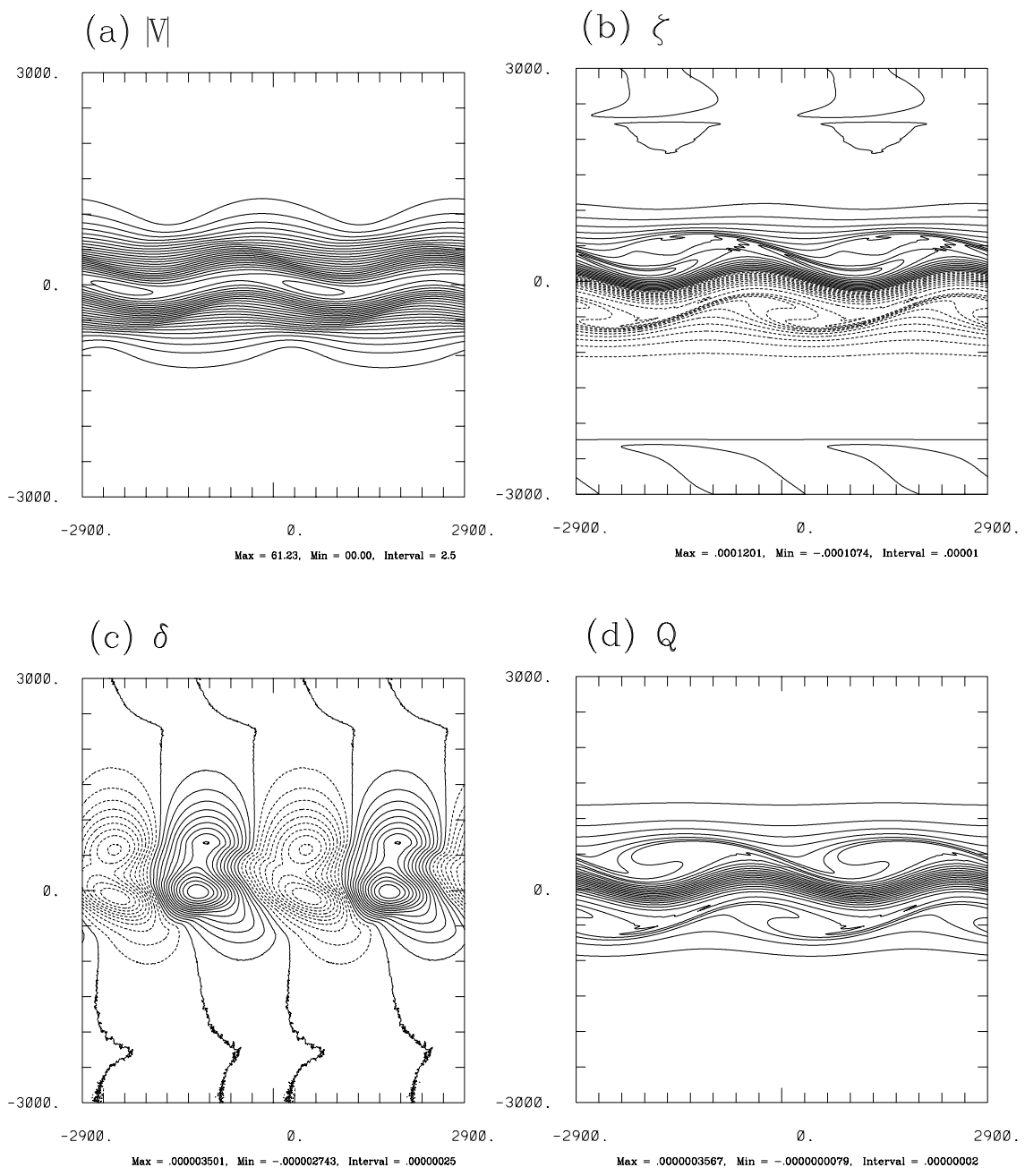


Figure 21: As in Fig. 20 but for $t = 110$ h.

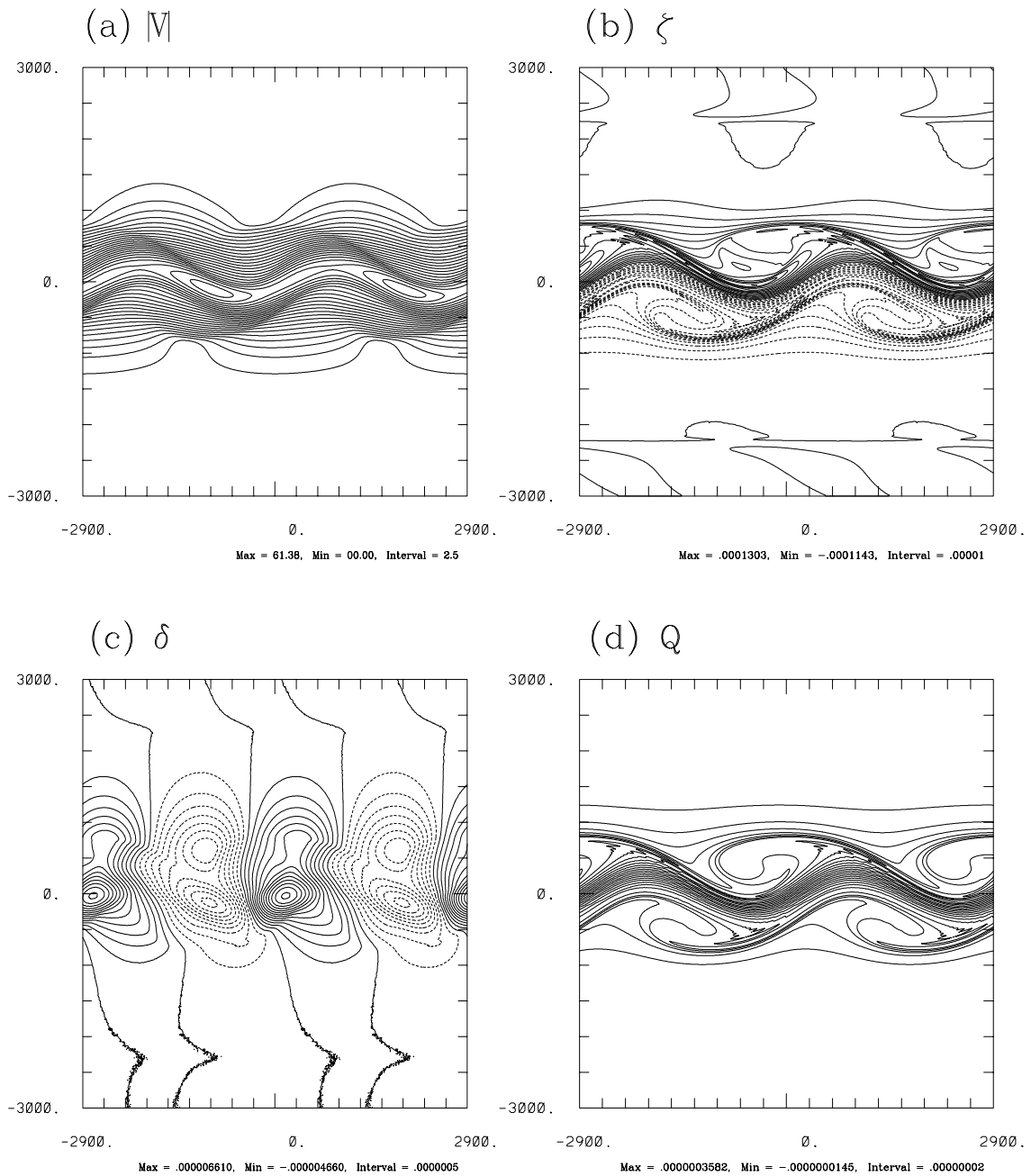


Figure 22: As in Fig. 20 but for $t = 130$ h.

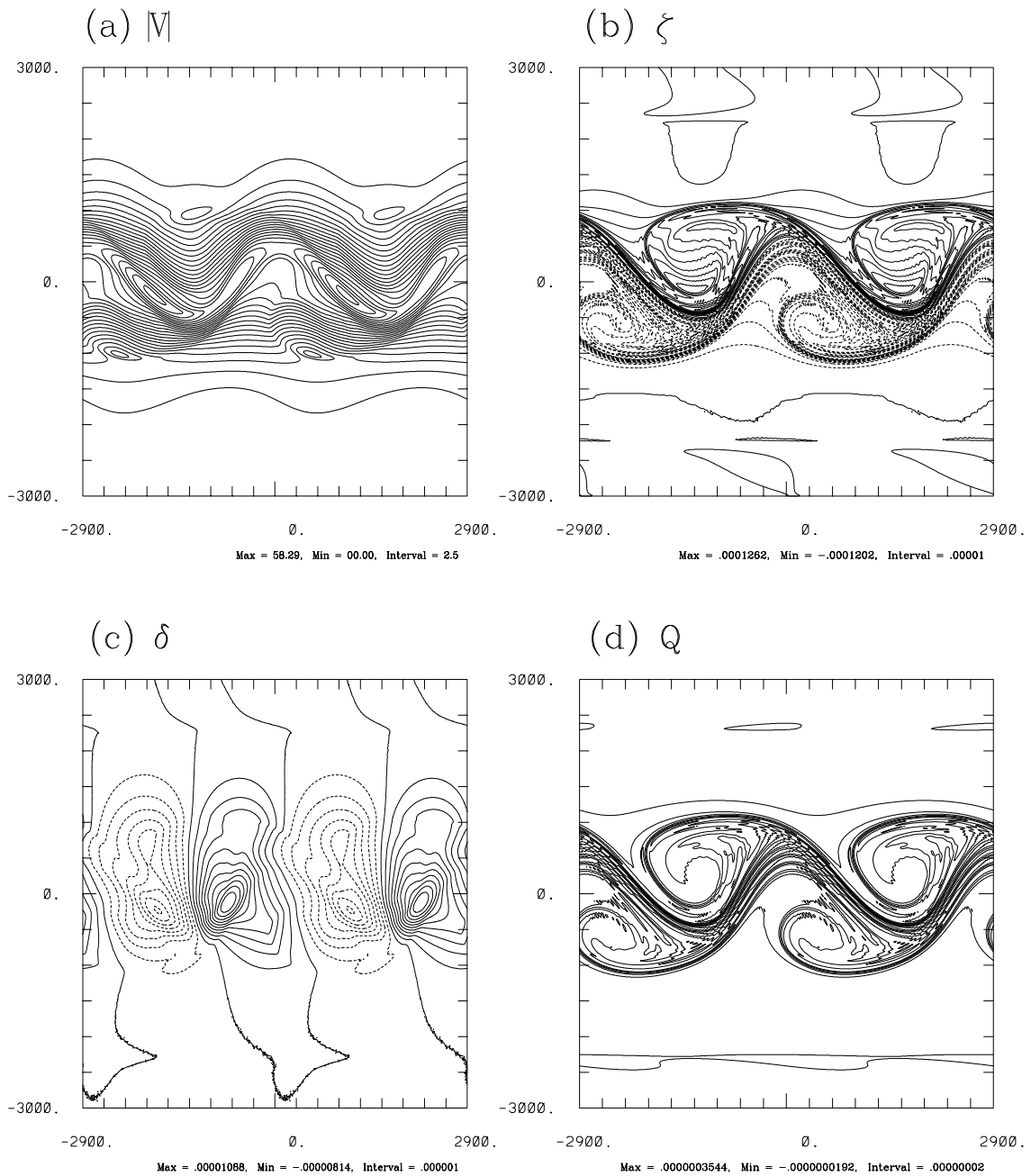
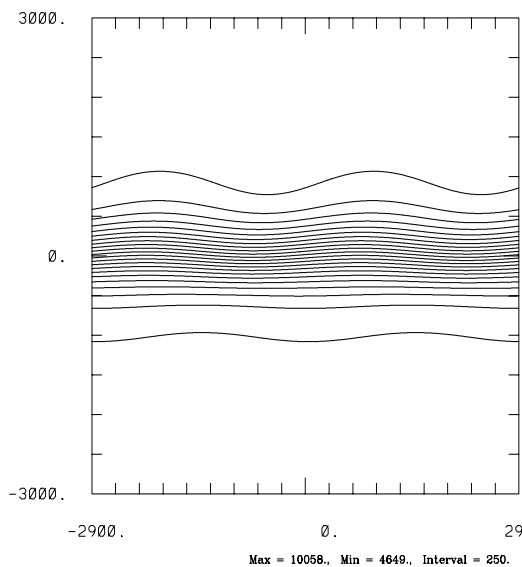
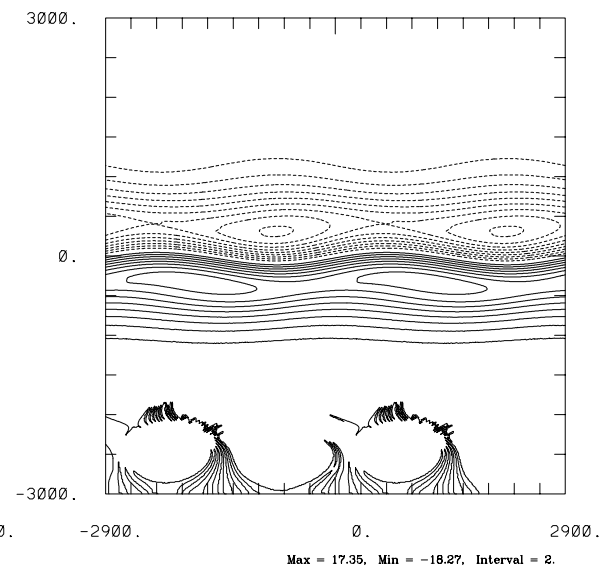


Figure 23: As in Fig. 20 but for $t = 150$ h.

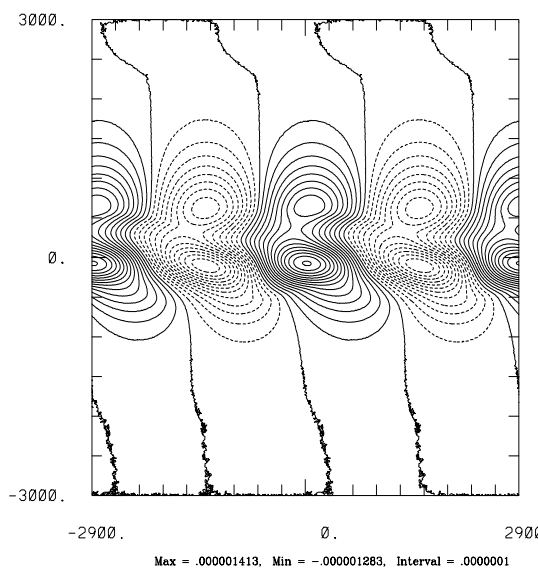
(a) Balanced Φ



(b) Unbalanced Φ



(c) Balanced δ



(d) Unbalanced δ

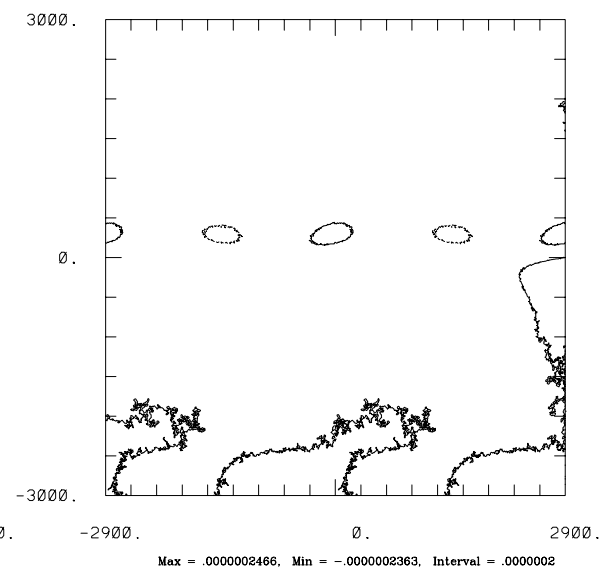
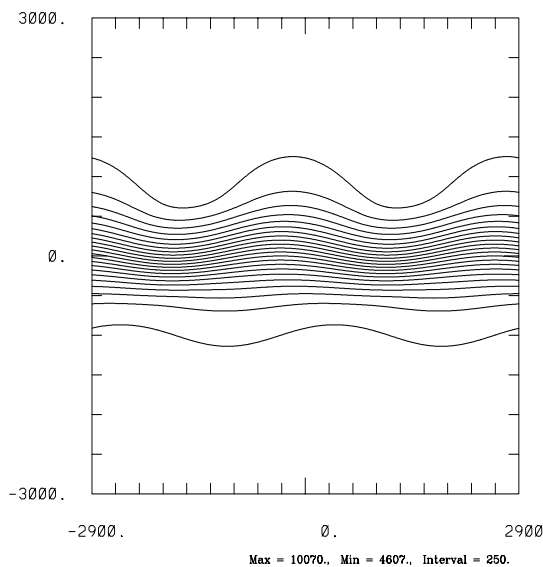
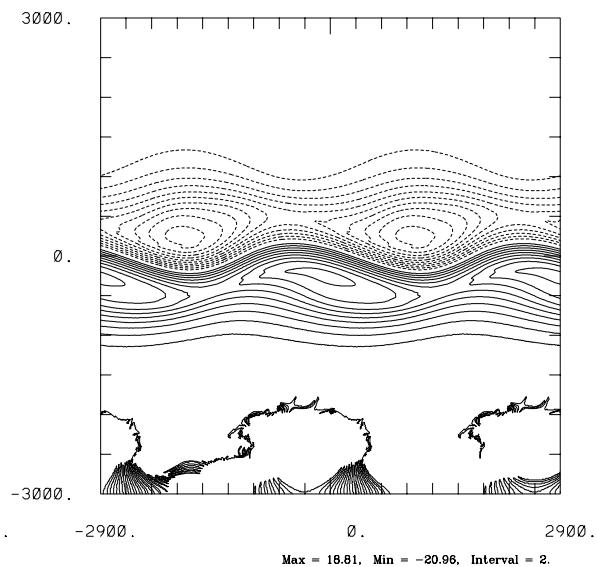


Figure 24: Balanced and unbalanced geopotential height ($\text{m}^2 \text{s}^{-2}$) and horizontal divergence (s^{-1}) plots for $t = 90 \text{ h}$.

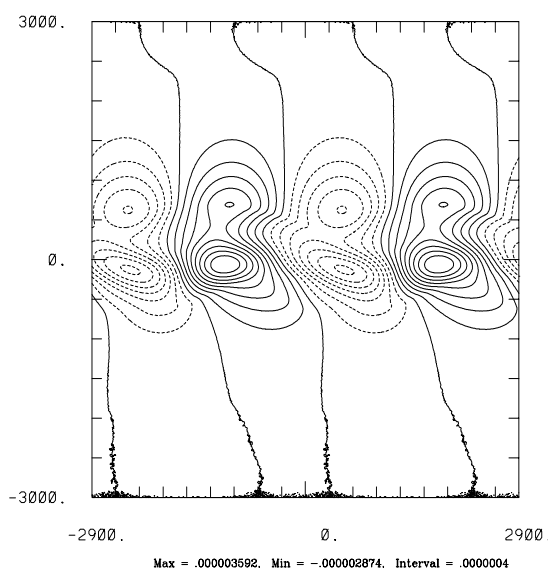
(a) Balanced Φ



(b) Unbalanced Φ



(c) Balanced δ



(d) Unbalanced δ

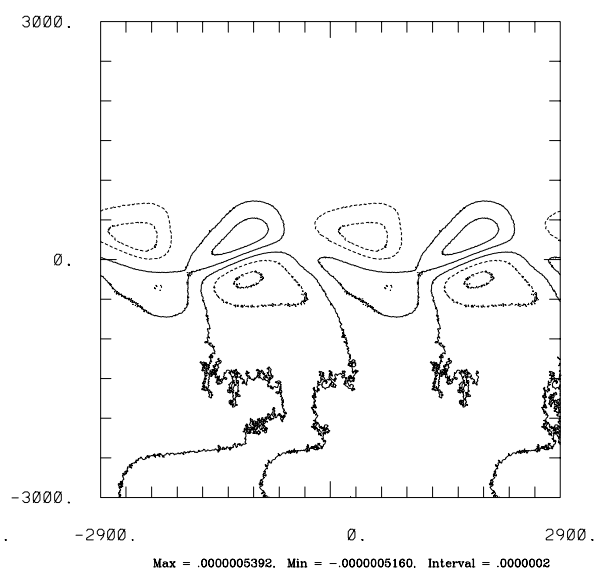
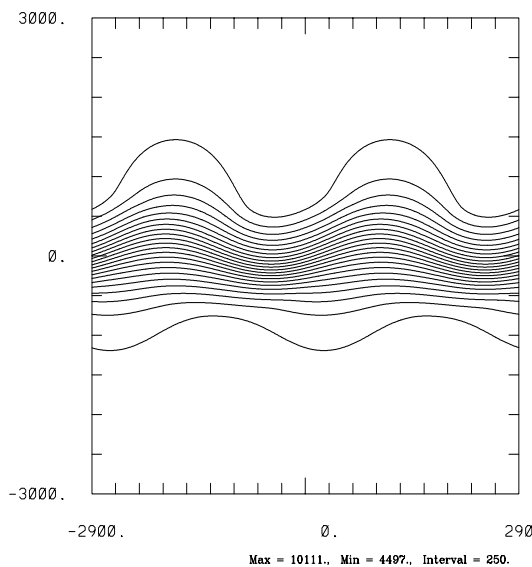
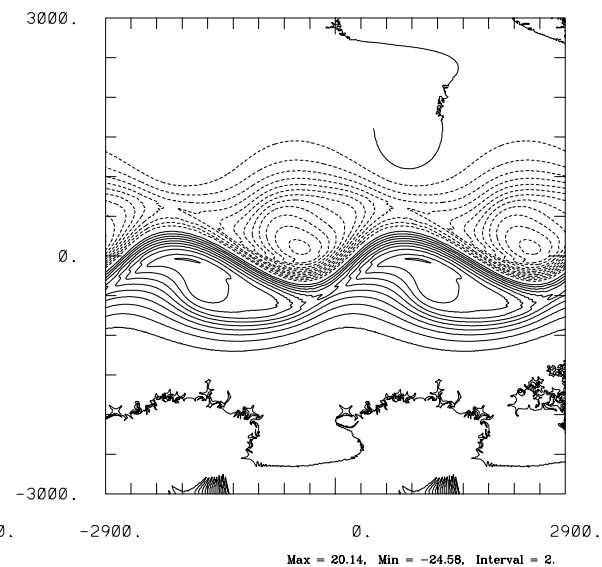


Figure 25: As in Fig. 24 but for $t = 110$ h.

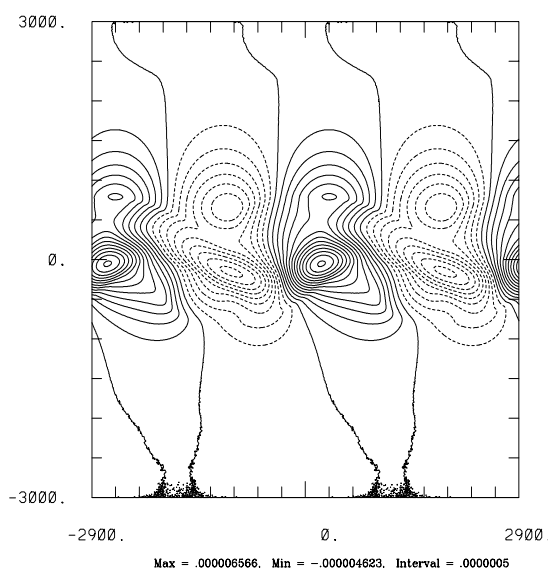
(a) Balanced Φ



(b) Unbalanced Φ



(c) Balanced δ



(d) Unbalanced δ

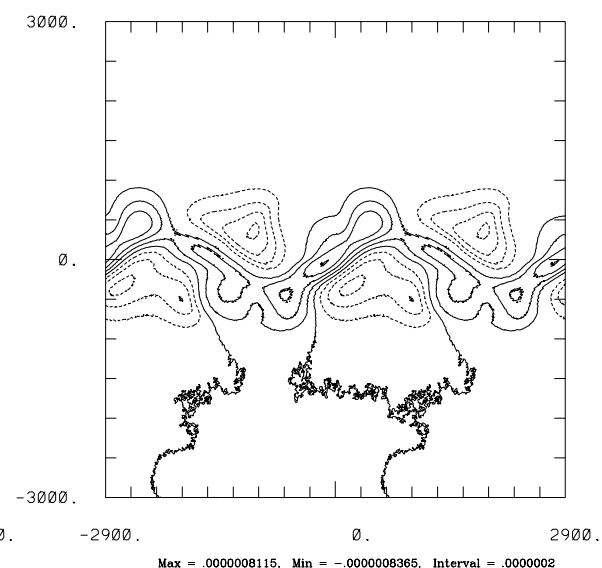
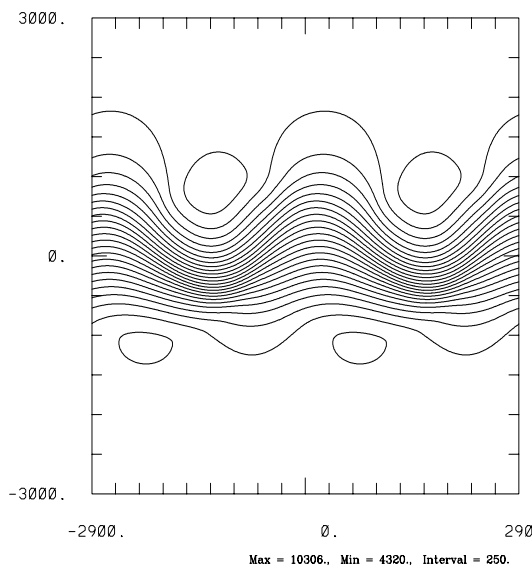
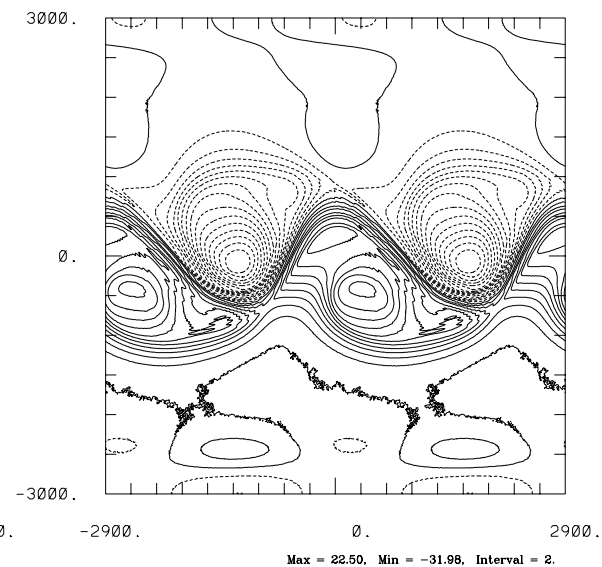


Figure 26: As in Fig. 24 but for $t = 130$ h.

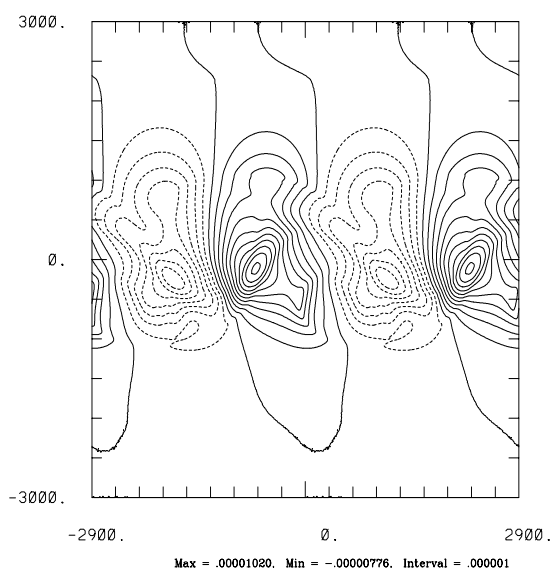
(a) Balanced Φ



(b) Unbalanced Φ



(c) Balanced δ



(d) Unbalanced δ

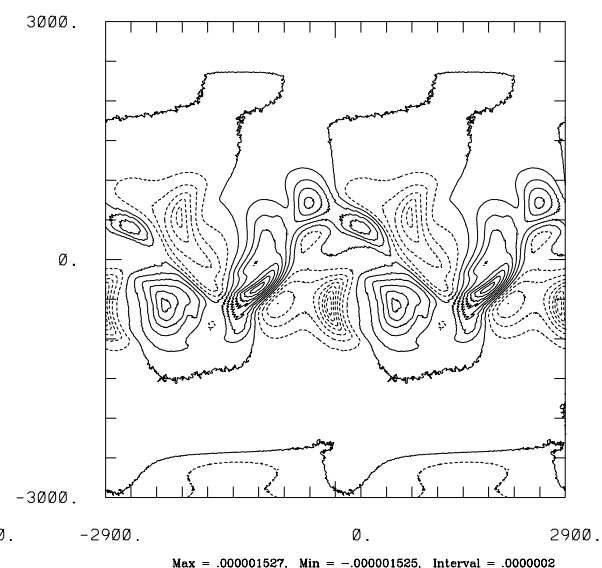


Figure 27: As in Fig. 24 but for $t = 150$ h.

Table III. Summary of all diagnostic calculations and PV inversion results for each simulation.

Diagnostic Calculation	$U_o = 20 \text{ m s}^{-1}; y_o = 600 \text{ km}$	$U_o = 30 \text{ m s}^{-1}; y_o = 450 \text{ km}$	$U_o = 60 \text{ m s}^{-1}; y_o = 450 \text{ km}$
Ro_J	0.20	0.70	1.33
Fr_J	0.17	0.35	0.70
Max. divergence (s^{-1})	$O(10^{-6})$	$O(10^{-6})$	$O(10^{-5})$
Max. vorticity (s^{-1})	$O(10^{-5})$	$O(10^{-4})$	$O(10^{-4})$
Max. local Ro	0.32	0.65	1.3
Max. local Fr	0.32	0.36	0.71
Max. gamma	$O(10^{-2})$	$O(10^{-2})$	$O(10^{-1})$
Max. div. Tendency (s^{-2})	$O(10^{-10})$	$O(10^{-10})$	$O(10^{-10})$
Max. Ro_L	0.06	0.17	0.31
Max. growth rate (J s^{-1})	$2.3 * 10^{-6}$	$5.2 * 10^{-6}$	$0.7 * 10^{-5}$
Max. bal. geopotential (m)	$O(10^4)$	$O(10^4)$	$O(10^4)$
Max. bal. divergence (s^{-1})	$O(10^6)$	$O(10^6)$	$O(10^5)$
Max. unbal. geopotential (m)	$O(1)$	$O(10)$	$O(10)$
Max. unbal. divergence (s^{-1})	$O(10^{-8})$	$O(10^{-7})$	$O(10^{-6})$

CHAPTER FOUR

SUMMARY AND CONCLUSIONS

The simulations shown here represent an exploration of the evolution of balance in both weak and strong initially balanced zonal barotropic jets on an f plane using a one-layer shallow-water equation model. Even though this study does not present an exact definition of balance, it provides insight on its evolution throughout the life cycle of barotropic instability. Again, the central question of this thesis is how do jets that are initially in balance evolve towards an unbalanced state and generate IGWs and when does that imbalance occur over the evolution of the life cycle of an unstable wave. This study utilizes very high resolution (10 km in both x and y) to present the evolution of balanced and unbalanced flow in a barotropic shallow-water model. Both the jet wind speed and width are chosen to produce simulations in which the instabilities of the wave growth are compared and contrasted with each simulation ranging from low Ro and Fr number to large Ro nor Fr number.

Several diagnostic calculations are utilized (local Rossby and Froude number, Lagrangian Rossby number, ratio of horizontal divergence to relative vorticity, large values of horizontal divergence and its material derivative, and PV inversion) to attempt to resolve the instance in which balance breaks down and subsequent inertia-gravity wave activity occurs. The results of the diagnostic calculations reveal that nonlinear balance is essentially valid for this particular jet structure, even though the Rossby and Froude numbers are both $O(1)$ in several of the simulations. This is contradictory to scale analysis (e.g., McWilliams 1985; Spall and McWilliams 1992), where it is required that either Ro or Fr be small for nonlinear balance to be valid. Even though McIntyre and Norton (2000) found that gravity wave activity of large amplitude was generally not

found in the integration of the shallow-water equations for large Ro number, they were unable to completely rule them out due to the resolution used in the model.

The evolution of the maximum local Ro number throughout each simulation shows that it only increases slightly as the barotropic wave grows. The maximum local Froude number remains essentially the same throughout the simulations because the jet speed does not vary greatly. The Lagrangian Rossby number, the ratio of the magnitude of the ageostrophic wind to the magnitude of the total wind, is calculated, and unbalanced flow tends to develop in regions in which large ageostrophic motions are occurring. Van Tuyl and Young (1982) found in numerical simulations that the Lagrangian Rossby number is typically greater than 0.5 in regions of unbalanced flow. The largest values of Ro_L occur in the simulations in which the Ro and Fr number is $O(1)$; however, these values only range from 0.2 to 0.3 at their maximum. The evolution of the parameter, γ , shows that it remains less than $O(10^{-1})$ for the duration of each simulation, such that the maximum horizontal divergence remains small in comparison to the maximum relative vorticity. This implies that nonlinear balance should remain valid to a good approximation throughout each simulation, despite the fact that neither the Rossby nor the Froude numbers are small enough to suggest a priori that this should be the case. This implication is also substantiated by evaluating the terms in the divergence equation that are neglected, namely the divergence tendency and advection of divergence terms. Such terms remain small throughout each simulation (i.e., $\leq 10^{-10} \text{ s}^{-2}$ and $\leq 10^{-12} \text{ s}^{-2}$ respectively), suggesting that IGW wave activity is negligible in these cases.

However, to further understand and test these diagnostic results, it is imperative to show the evolution of balanced and unbalanced flows through the utility of potential vorticity inversion. In their landmark paper, Hoskins et. al. (1985) stated that the “invertibility principle” of PV, given a suitable balance condition, allows for the total mass, wind, and all other dynamical fields to be deduced knowing the global distribution of PV. Using the property that the fast modes or gravity wave modes in the shallow-water equations have zero linearized potential vorticity, it is possible to elucidate the balanced and unbalanced fields based on the PV field. Essentially, the PV field is a completely balanced entity and the balanced dynamical fields can be obtained from the total dynamical fields.

The PV inversion used in this study is derived from a set of equations introduced by Lynch (1989) in which the fast modes are filtered from the shallow-water equations by eliminating the divergence tendency and the tendency of geostrophic imbalance. The results of the PV inversion applied to each simulation indicate that the initially balanced flows eventually attain a certain amount of imbalance as the unstable wave grows. As the jet and the wave evolve, unbalanced structures become readily apparent in the unbalanced fields. However, it is important to examine the magnitude of the imbalance, not only the structure, to correctly diagnose whether the flow is in a state of imbalance. In each simulation, the maximum values of unbalanced geopotential height occur in the vicinity of the greatest maximum jet wind speeds. The absolute maximum unbalanced divergence values occur in the highly curved flow region just downstream from the jet streak; however, there are several centers of secondary, but smaller, maxima associated with the various regions of parcel acceleration and curvature throughout the vicinity of the jet. This agrees with observational and numerical studies in literature suggest that IGWs are generated in the vicinity of jets and fronts in the upper troposphere. In particular, Uccellini and Koch (1987) found that IGWs typically develop in a region of unbalanced flow in the exit region of an upper-level jet streak given that the atmosphere is statically stable throughout. The imbalance tends to occur in regions of large air parcel deceleration and in regions of curved flow, so the results of the PV inversion for each simulation appear to be correct in a physical sense.

The largest magnitude of unbalanced geopotential and divergence occurs in the simulation in which both the Ro and Fr number are $O(1)$. This result makes sense, especially in terms of scale analysis, in which the divergence terms in the divergence equation should be of some significance. However, the magnitude of the unbalanced divergence is quite small compared to the total divergence. For the simulation in which the Ro and Fr numbers are both $O(1)$, the magnitude of the unbalanced divergence is generally 10% of the total divergence. The magnitudes for the other simulations were generally less than 10% of the total divergence. It has been shown in numerical simulations of IGWs that the unbalanced divergence can be of similar magnitude to the total divergence. These results compliment the earlier diagnostic calculations, showing that IGW activity is non-existent or very limited in these barotropic shallow-water

equation simulations. The PV inversion ultimately reveals that nonlinear balance is essentially valid for the barotropic shallow-water model simulations.

Even though the presence of unbalanced flow, either in numerical simulations or in atmospheric data, is typically inferred via the various diagnostic quantities in this study, it is possible that these quantities may not totally describe the nature of the imbalance. These quantities are based on specific balance constraints (i.e., quasigeostrophy, semigeostrophy, or nonlinear balance), and it should be noted that an assessment of balance based on the inaccuracy of these constraints admits the possibility that the unbalanced flow so identified may include higher-order motion not accounted for in the system under consideration in addition to IGWs. Even though the results of this study indicate the magnitude of the imbalance is quite small, an ad hoc calculation of the second order derivative of the divergence tendency also indicated that higher-order balanced motions were unlikely present in the simulations. The higher-order divergence tendency fields essentially showed no structure at all in these simulations.

There are few possible limiting factors to the generation of IGWs in the shallow water model. There is a possibility that, in the shallow-water system, there is a constraint on the growth of the mean-square divergence that may limit the potential for gravity wave generation and/or amplification. Also, possible effects of the time filter (Asselin) may be important. If the time filter coefficient is set too high, IGWs may be damped quite an extent. To test the filter, implementation of an initially unbalanced simulation initiated continuous gravity wave propagation from the jet region. In general, the IGWs generally were not greatly affected by the filter as they radiated from the jet region, and the filter would have little bearing on IGWs that may have developed in the simulations.

Reserching the potential impacts on the present study due to the addition of such factors as topography, beta-effect, and baroclinicity also should provide insight on the generation of unbalanced flow and IGWs. In the real atmosphere, topography sometimes forces the flow to become unbalanced and produce gravity waves and the addition of topography to this model may force IGW formation. Through scale analysis, the beta effect is extremely small compared to the Coriolis effect and should have little effect on the results. A baroclinic or multi-layer atmosphere allows for faster conversion of available potential energy to kinetic energy resulting in a more rapid development of the

dynamical fields associated with an unstable wave. Growth rates associated with a baroclinic atmosphere are greater than for a barotropic atmosphere, and gravity wave structures or signals are more likely to develop (which has been shown by many investigators), especially with regards to structures within the jet itself. Also, the addition of a stratosphere to the model would enable IGWs to propagate vertically and increase in amplitude with height due to the density changes associated with stratification.

Ongoing and future research in the study of balance evolution is very important if we are ever to understand what is meant by “balance”. Applying the various diagnostic calculations and techniques discussed in the study to a baroclinic wave life cycle is the next logical step in obtaining an increased understanding of the evolution of unbalanced flow. Also, exploring the possibility of employing the higher-order potential vorticity inversion techniques described by McIntyre and Norton (2000) to identify imbalance in the vicinity of the jet, along with the methodology employed by Ford (1994) to identify IGW activity in the far field will be very helpful in simulations in which IGW are readily apparent. Expanding the study to include other models and different jet structures are also a possibility to gain much greater insight in IGW formation.

The calculations and techniques described in this study are ad hoc; however, they provide the necessary means to begin to diagnose unbalanced flow and IGW formation in numerical simulations and in atmospheric data. The barotropic shallow-water model is the simplest non-trivial dynamical framework in which balanced and unbalanced flow can coexist; therefore, it is sensible to begin with this model and expand the study to more complicated regimes. In other words, a hierarchical approach should be taken by building upon simpler dynamical frameworks. The study of IGWs and unbalanced flow is quite difficult; however, more studies are needed in order to gain a more complete understanding of the dynamics of the atmosphere and its motions.

REFERENCES

- Allen, J. S., J. A. Barth, and P. A. Newberger, 1990: On intermediate models for barotropic continental shelf and slope flow fields. Part I: Formulation and comparison of Exact Solutions. *J. Phys. Ocean.*, **20**, 1017-1043.
- Arakawa, A., 1966: Computational design for long-term numerical integrations of the Equations of atmospheric motion. *J. Comput. Phys.*, **1**, 119-143.
- Arakawa, A. and V. R. Lamb, 1981: A potential enstrophy and energy conserving scheme for the shallow water equations. *Mon. Wea. Rev.*, **109**, 18-36.
- Bartello, P., 1995: Geostrophic adjustment and inverse cascades in rotating stratified turbulence. *J. Atmos. Sci.*, **52**, 4410-4428.
- Blumen, W., 1972: Geostrophic adjustment. *Rev. Geophys. Space Phys.*, **10**, 485-328.
- Bosart, L. F., W. E. Bracken, and A. Seimon, 1998: A study of cyclone mesoscale Structure with emphasis on a large-amplitude inertia-gravity wave. *Mon. Wea. Rev.*, **126**, 1497-1527.
- Bush, A. B. G., J. C. McWilliams, and W. R. Peltier, 1995: Origins and evolution of imbalance in synoptic-scale baroclinic life cycles. *J. Atmos. Sci.*, **52**, 1051-1069.
- Charney, J. G., 1948: On the scale of atmospheric motions. *Geof. Publ.*, **17**, 3-17.
- Charney, J. G., R. Fjörtoft, and J. von Neumann, 1950: Numerical integration of the barotropic vorticity equation. *Tellus*, **2**, 237-254.
- Charney, J. G., 1962: Integration of the primitive and balance equations. *Proc. Int. Symp. on Numerical Weather Prediction*, Tokyo, Japan, Meteor. Soc. Japan, 131-152.
- Charron, M., and G. Brunet, 1999: Gravity wave diagnosis using empirical normal modes. *J. Atmos. Sci.*, **56**, 2706-2727.
- Cunningham, P., 1997: Analytical and numerical modeling of jet-streak dynamics. Master's Thesis, State University of New York at Albany, 150 pp.
- Davis, C. A. and K. A. Emanuel, 1991: Potential vorticity diagnostics of cyclogenesis. *Mon. Wea. Rev.*, **119**, 1929-1953.

- Davis, C. A., and M. L. Weisman, 1994: Balanced dynamics of mesoscale vortices in simulated convective systems. *J. Atmos. Sci.*, **51**, 2005-2030.
- Davis, C. A., E. Donall Grell, and M. A. Shapiro, 1996: The balanced dynamical nature of a rapidly intensifying oceanic cyclone. *Mon. Wea. Rev.*, **124**, 3-26.
- Dritschel, D. G., and M. H. P. Ambaum, 1997: A contour-advection semi-Lagrangian numerical algorithm for simulating fine-scale conservative dynamical fields. *Q. J. R. Meteorol. Soc.*, **123**, 1097-1130.
- Errico, R. M., 1982: Normal mode initialization and the generation of gravity waves by quasi-geostrophic forcing. *J. Atmos. Sci.*, **39**, 574-586.
- Errico, R. M., 1984: The dynamical balance of a general circulation model. *Mon. Wea. Rev.*, **112**, 2439-2454.
- Ford, R., 1994: The instability of an axisymmetric vortex with monotonic potential vorticity in rotating shallow water. *J. Fluid Mech.*, **280**, 303-334.
- Ford, R., M. E. McIntyre, and W. A. Norton, 2000: Balance and the slow quasimaniold: some explicit results. *J. Atmos. Sci.*, **57**, 1236-1254.
- Fritts, D. C., M. A. Geller, B. B. Balsley, M. L. Chanin, I. Hirota, J. R. Holton, S. Kato, R. S. Lindzen, M. R. Schoeberl, R. A. Vincent, and R. F. Woodman, 1984: Research status and recommendations from the Alaska workshop on gravity waves and turbulence in the middle atmosphere, Fairbanks, Alaska, 18-22 July 1983. *Bull. Amer. Meteor. Soc.*, **65**, 149-159.
- Fritts, D. C., and H.-G. Chou, 1987: An investigation of the vertical wavenumber and frequency spectra of gravity wave motions in the lower stratosphere. *J. Atmos. Sci.*, **44**, 3610-3624.
- Fritts, D. C., T. Toshitaka, T. E. VanZandt, S. A. Smith, T. Sato, S. Fukao, and S. Kato, 1990: Studies of velocity fluctuations in the lower atmosphere using the MU radar. Part II: Momentum fluxes and energy densities. *J. Atmos. Sci.*, **47**, 51-66.
- Fritts, D. and Z. Luo, 1992: Gravity wave excitation by geostrophic adjustment of the jet stream. Part I: Two-dimensional forcing. *J. Atmos. Sci.*, **49**, 681-697.
- Fritts, D. C. and T. E. Vanzandt, 1993: Spectral estimates of gravity wave energy and momentum fluxes. Part I: Energy dissipation, acceleration, and constraints. *J. Atmos. Sci.*, **50**, 3685-3694.
- Fritts, D. C., D. M. Riggan, B. B. Balsey, and R. G. Stockwell, 1998. Recent results with an MF radar at McMurdo, Antarctica: Characteristics and variability of motions

- near 12-hour period in the mesosphere. *Geophys. Res. Lett.*, **25**, 297-300.
- Garnier, E., O. Metais, and M. Lesieur, 1998. Synoptic and frontal-cyclone instabilities in baroclinic jet flows. *J. Atmos. Sci.*, **55**, 1316-1335.
- Guest, F. M., M. J. Reeder, C. J. Marks, and D. J. Karoly, 2000: Inertia-gravity waves observed in the lower stratosphere over Macquarie Island. *J. Atmos. Sci.*, **57**, 737-752.
- Haltiner, G.J. and R. T. Williams, 1980: *Numerical Prediction and Dynamic Meteorology*. John Wiley & Sons, 417 pp.
- Hirota, I., and T. Niki, 1986: A statistical study of inertia-gravity waves in the middle atmosphere. *J. Meteor. Soc. Japan*, **63**, 995-999.
- Holton, J. R., 1983: The influence of gravity wave breaking on the general circulation of the middle atmosphere. *J. Atmos. Sci.*, **40**, 2497-2507.
- Hoskins, B.J., M. E. McIntyre, and A. W. Robertson, 1985: On the use and significance of isentropic potential vorticity maps. *Quart. J. Roy. Meteor. Soc.*, **111**, 877-946.
- Jiang, H., and D. J. Raymond, 1995: Simulation of a mature mesoscale convective system using a nonlinear balance model. *J. Atmos. Sci.*, **52**, 161-175.
- Kaplan, M. L., and D. A. Paine, 1977: The observed divergence of the horizontal velocity field and pressure gradient force at the mesoscale; its implications for the parameterization of three-dimensional momentum transport in synoptic scale numerical models. *Contrib. Atmos. Phys.*, **50**, 321-330.
- Kaplan, M. L., S. E. Koch, Y. Lin, R. P. Weglarz, and R. A. Rozumalski, 1997: Numerical simulations of a gravity wave event over CCOPE. Part I: The role of geostrophic adjustment in mesoscale jetlet formation. *Mon. Wea. Rev.*, **125**, 1185-1211.
- Koch, S. E. and R. E. Golus, and P. B. Dorian, 1988: A mesoscale gravity wave event observed during CCOPE. Part II: Interactions between mesoscale convective systems and antecedent waves. *Mon. Wea. Rev.*, **116**, 2545-2569.
- Koch, S. E. and P. B. Dorian, 1988: A mesoscale gravity wave event observed during CCOPE. Part III: wave environment and probable source mechanisms. *Mon. Wea. Rev.*, **116**, 2570-2592.
- Koppel, L. L., L. F. Bosart, and D. Keyser, 2000: A 25-yr climatology of large-amplitude hourly surface pressure changes over the conterminous United States. *Mon. Wea. Rev.*, **128**, 51-68.

- Leith, C. E., 1980: Nonlinear normal mode initialization and quasi-geostrophic theory. *J. Atmos. Sci.*, **37**, 958-968.
- Lorenz, E. N., 1960. Maximum simplification of the dynamic equations. *Tellus*, **12**, 243-254.
- Lorenz, E. N., 1980: Attractor sets and quasi-geostrophic equilibrium. *J. Atmos. Sci.*, **37**, 1685-1699.
- Lynch, Peter, 1989: The slow equations. *Quart. J. Roy. Meteor. Soc.*, **115**, 201-219.
- Luo, Z. and D. C. Fritts, 1993: Gravity-wave excitation by geostrophic adjustment of the jet stream. Part II: Three-dimensional forcing. *J. Atmos. Sci.*, **50**, 104-115.
- Matsuno, T., 1982: A quasi one-dimensional model of the middle atmospheric circulation interacting with internal gravity waves. *J. Meteor. Soc. Japan*, **60**, 215-226.
- McIntyre, M. E. and W. A. Norton, 2000: Potential vorticity inversion on a hemisphere. *J. Atmos. Sci.*, **57**, 1214-1235.
- McWilliams, J. C., 1985: A uniformly valid model spanning the regimes of geostrophic and isotropic, stratified turbulence: Balance turbulence. *J. Atmos. Sci.*, **42**, 1773-1774.
- Mohebalhojeh, A. and D. Dritschel, 2000: On the representation of gravity waves in numerical models of the shallow-water equations. *Quart. J. Roy. Meteor. Soc.*, **126**, 669-688.
- Mohebalhojeh, A. and D. Dritschel, 2001: Hierarchies of balance conditions for the f-plane shallow-water equations. *J. Atmos. Sci.*, **58**, 2411-2426.
- Montgomery, M. T., and B. F. Farrell, 1992: Polar low dynamics. *J. Atmos. Sci.*, **49**, 2484-2505.
- Moore, J. T., and W. A. Abeling, 1988: A diagnostic of unbalanced flow in upper levels during the AVE-SESAME I period. *Mon. Wea. Rev.*, **116**, 2424-2436.
- Olsson, P. Q., and W. R. Cotton, 1997: Balanced and unbalanced circulations in a primitive equation simulation of a midlatitude MCC. Part II: Analysis of balance. *J. Atmos. Sci.*, **52**, 479-497.
- O'Sullivan, D. and T. J. Dunkerton, 1995. Generation of inertia-gravity waves in a simulated life cycle of baroclinic instability. *J. Atmos. Sci.*, **52**, 3695-3716.
- Sadourny, R., 1975: The dynamics of finite-difference models of the shallow-water equations. *J. Atmos. Sci.*, **32**, 680-689.

- Spall, M. A. and J. C. McWilliams, 1992: Rotational and gravitational influences on the degree of balance in the shallow-water equations. *Geophys. Astrophys. Fluid Dynamics.*, **64**, 1-29.
- Stobie, J. G., F. Einaudi, and L. W. Uccellini, 1983: A case study of gravity waves-convective storms interaction: 9 May 1979. *J. Atmos. Sci.*, **40**, 2804-2830.
- Uccellini, L. W., 1975: A case study of apparent gravity wave initiation of severe convective storms. *Mon. Wea. Rev.*, **103**, 497-513,
- Uccellini, L. W., and S. E. Koch, 1987: The synoptic setting and possible energy sources for mesoscale wave disturbances. *Mon. Wea. Rev.*, **115**, 721-729.
- Van Tuyl, A. H. and J. A. Young, 1982: Numerical simulation of nonlinear jet streak adjustment. *Mon. Wea. Rev.*, **110**, 2038-2054.
- Vautard, R., and B. Legras, 1986: Invariant manifolds, quasi-geostrophy and initialization. *J. Atmos. Sci.*, **43**, 565-584.
- Warn, T., 1986: Statistical mechanical equilibria of the shallow water equations. *Tellus*, **38A**, 1-11.
- Warn, T., 1997: Nonlinear balance and quasi-geostrophic sets. *Atmos. Ocean*, **35**, 135-145.
- Warn, T. and R. Menard, 1986: Nonlinear balance and gravity-inertial wave saturation in a simple atmospheric model. *Tellus*, **38A**, 285-294.
- Weglarz, R. P., and Y.-L. Lin, 1997: A linear theory for jet streak formation due to zonal momentum forcing in a stable stratified atmosphere. *J. Atmos. Sci.*, **54**, 908-932.
- Whitaker, J. S., 1993: A comparison of primitive and balance equation simulations of baroclinic waves. *J. Atmos. Sci.*, **50**, 1519-1530.
- Zack, J. W., and M. L. Kaplan, 1987: Numerical simulations of the subsynoptic features associated with the AVE-SESAME I case. Part I: The pre-convective environment. *Mon. Wea. Rev.*, **115**, 2367-2394.
- Zhang, F., 2004: Generation of mesoscale gravity waves in upper-tropospheric jet-front systems. *J. Atmos. Sci.*, **61**, 440-457.
- Zhang, F., and S. E. Koch, 2000: A survey of unbalanced flow diagnostics and their application. *Adv. Atmos. Sci.*, **17**, 165-183.
- Zhang, F., S. E. Koch, C. A. Davis, and M. L. Kaplan, 2001: Wavelet analysis and the

governing dynamics of a large-amplitude gravity wave event along the East coast of the United States. *Quart. J. Roy. Meteor. Soc.*, **127**, 2209-2245.

BIOGRAPHICAL SKETCH

Travis Allen Smith was born on May 12, 1978, in Wise, Virginia. He grew up in Big Stone Gap, Virginia, where he graduated from Powell Valley High School in 1996. He attended college at Virginia Polytechnic Institute and State University, where he obtained a Bachelor of Science degree in Chemical Engineering in 2001. While at Virginia Tech, he also participated in the cooperative education program, working for Honeywell, Inc. as a process engineer in Chesterfield, Virginia. Following his desire to study meteorology since he was a child, he enrolled in the Florida State University's Department of Meteorology in the Fall of 2001, completing the Master of Science degree in Summer, 2004. He plans to begin work on the Doctor of Philosophy degree in Meteorology in the Fall, 2004.